Can Wang, An Deng and Abbas Taheri

Digital image processing on segregation of rubber sand mixture

International Journal of Geomechanics, 2018; 18(10):04018138-1-04018138-13

Digital image processing on segregation of rubber sand mixture

Can Wang[1], An Deng[2], Abbas Taheri[3]

1. Graduate Student, School of Civil, Environmental and Mining Engineering, Univ. of Adelaide, Adelaide, SA 5005, Australia. E-mail: c.wang@adelaide.edu.au
2. Senior Lecturer, School of Civil, Environmental and Mining Engineering, Univ. of Adelaide, Adelaide, SA 5005, Australia (corresponding author). E-mail: an.deng@adelaide.edu.au
3. Senior Lecturer, School of Civil, Environmental and Mining Engineering, Univ. of Adelaide, Adelaide, SA 5005, Australia. E-mail: abbas.taheri@adelaide.edu.au

ABSTRACT

The segregation of rubber sand mixtures, when they form heaps as observed by the method of digital image processing (DIP), is presented. Through segmenting the digital images into a binary picture, the DIP method enables material ingredients identification and three-dimensional mapping of mixture segregation. This helps reach a better understanding of mixture heterogeneity when incorporating artificial material into conventional geotechnical materials. To gain an insight into the mixture heterogeneity, the DIP results were used to validate a discrete element model and the model was then used to examine the influence of particle properties on the segregation. The discrete element simulations showed that the particle density is critical in material segregation, and the segregation becomes more noticeable when the materials density ratio increases. This trend is restricted by increasing the inter-particle surface roughness.

Keywords: segregation; digital image processing; discrete element; density; roughness

INTRODUCTION

Waste tires create problems such as landfilling, health, and environmental challenges. The tires can go into recycling facilities for a new life. One of the new-life solutions is to reuse the tires as geomaterial alternatives (Foose et al. 1996; Zornberg et al. 2004). Rubber sand mixture is an attractive alternative and has been widely used in geotechnical applications, including roadway construction (Bosscher et al. 1997; Nightingale and Green 1997), lightweight fill (Ahmed and Lovell 1993; Masad et al. 1996), backfill for retaining walls (Humphrey and Manion 1992; Garga and O'shaughnessy 2000), slope stabilization (Poh and Broms 1995) and seismic isolation system (Tsang et al. 2012). Where the mixtures are prepared, placed or compacted, the ingredients likely segregate. Whichever induces the material segregation, a segregated profile causes heterogeneity and sometimes severe instability problems such as liquefaction (Yoshimine and Koike 2005). The sand and rubber ingredients differ at least in density and surface roughness and, when placed as a mixture, lead to flow-induced segregation as defined by Ottino and Khakhar (2000). In general, the factors causing segregation can be classified into particle sizes, densities, shapes and particle resilience (Williams 1976). Of all the segregation mechanisms, trajectory segregation, percolation of fine particles and the rise of coarse particles on vibration are commonly recognized (Kudrolli 2004). Other mechanisms such as rolling, sieving, water flow, soil crushing etc. were also reported in early works (Kuerbis and Vaid 1988; Ottino and Khakhar 2000; Lőrincz et al. 2005; Watabe et al. 2014).

The first reported work on segregation mechanism came from Donald and Roseman (1962), who investigated the experiment of mixing particles of different sizes and densities in a rotating horizontal drum. The recent work to study segregation by using the discrete element method (DEM) has become popular as the DEM is regarded as a valuable tool for studying granular flow and mixing mechanisms, e.g., free surface (Shi et al. 2007) and hopper discharge (Anand et al. 2010). These tests have shown unanimously that the particle size and density are the major factors leading to segregation. Other factors, such as shape, chute angle, liquid content, rolling friction and magnetic fields also contribute to material segregation (Anand et al. 2010).

While extensive studies have been performed to test material segregation, there is limited research regarding segregation phenomenon when the rubber sand mixture falls to form a heap. There is also a limited quantitative connection in terms of segregation measurements between numerical simulations and experimental observation. Studies of the sand pile by DEM simulation are limited when it comes to the angle of repose or force of percolation (Zhou et al. 1999; Yang et al. 2000; Zhou et al. 2001). And although significant achievements have been made since Zhou et al. (1999) first introduced the concept ‘rolling friction’ in studying heap formation, there is a lack of study regarding the phenomenon of segregation.

This paper presents the segregation phenomenon observed when the rubber sand forms a heap. It investigates the influence of particle properties using DEM. Since many studies have been conducted on evaluating particle sizes, this paper focused on studying segregation without size difference, e.g., a mixture with similar ingredient sizes. The results of the study are presented as a comparison between experiments and numerical simulations so that a parametric study can be performed. Also, it contains the calibration process for restitution coefficient measurements and the angle of repose tests so that important micro-properties could be obtained. These examinations help quantify mixture segregation when the mixture is processed. The parametric study will examine and identify the critical material properties causing the segregation and whereby solutions can be recommended to reduce the segregation.

METHODOLOGY

In this section, prior to investigating material segregation, a number of tests are performed to study granular behavior. DEM is adopted as a numerical method to calibrate micromechanical properties. This could be achieved through heap-forming test and repose angle studies. Serious segregation was identified in the mixture pile after the heap-forming process in both numerical simulation and tests. To accurately measure the material segregation, digital image processing is used. Detailed discussion will be provided in the following sections.

Discrete Element Method

To simulate the granular interaction, the use of DEM can provide an insight into the micromechanical properties reflecting the macroscopic phenomenon. This method simulates the material as a collection of frictional and rigid spheres so that complex problems can be addressed through observing particles contact (Cundall and Strack 1979). The contact model, as depicted in Itasca (2009), is shown in Figure 1. The contact model can be treated as either a linear model or as a non-linear model (e.g., Hertz–Mindlin contact). Both models produce normal and shear forces based on normal contact and shear stiffness respectively. A Coulomb limit is imposed on the shear force considering a friction coefficient, u. The dashpot component is assumed to dissipate extra energy in both normal and shear directions.

Damping Ratio

As a part of an examination of the microscopic properties, it is necessary to evaluate the effect of material damping which could have an impact on mixture segregation. The damping ratio is a dimensionless parameter that quantifies system decay during oscillations, which is an important property input in DEM. Also, for a numerical analysis on rubber sand mixture, the individual damping ratio at granular contact is not clear and lacks a calibration process

(Patil et al. 2010; Evans and Valdes 2011; Lee et al. 2014). In the repose angle test, when different particles are dropped from a height, due to the difference in granular re-bound height, it may generate a different heap when they are stabilized, which may greatly influence the mixture segregation at its surface. Therefore, calibrating the material damping ratio as a DEM input parameter is necessary. According to Kawaguchi et al. (1992), the restitution height is directly linked to the material properties of energy dissipation, and the relationship can be obtained by solving the motion equation for free vibration with viscous damping, as follows:

$$\alpha = \exp\left(-\frac{\zeta\pi}{\sqrt{1-\zeta^2}}\right) \quad (1)$$

where α is restitution coefficient which is determined from the restitution height, h; ζ is the ratio of the damping constant to the critical damping constant. For simplification, ζ is referred to as the 'damping ratio'. It is clear that a granule's damping ratio can be calculated through its re-bound height. Therefore, an experiment was designed to calibrate this parameter input.

The materials used for the experiment were spherical silica beads and rubber beads with a radius of 5 mm, as shown in Figure 2. The two materials are identical in composition respectively to the sand and rubber beads used for the mixture. The restitution process used a glass board as a base. Silica and rubber beads were released at a height of H=340 mm, against a vertical scale board, and a high resolution camera of 60 fps was placed one meter in front of the scale board. The material size and the release height were determined as being proportional to the sizes of samples used for the tests that followed.

Four silica and four rubber beads were chosen at random for the test, as shown in Figure 2. Each silica and rubber bead was tested three times independently. Once the beads were released the maximum re-bound height was captured by using the camera to record the whole process, as shown in Figure 3. The images were analyzed at each frame so that the maximum restitution height could be determined. The material beads at the maximum re-bouncing height are illustrated in Figure 3. The final results of the repeated tests are given in Figure 4. Generally, the silica beads had a much higher height of bounce, with an average of 170 mm. Rubber beads rebound to 31.9 mm on average.

For both of the silica and rubber beads, the radius of the bead, r=5 mm, must be deducted when comparing its height of rebound. Therefore the restitution coefficient α is expressed as:

$$\alpha = \frac{h - r}{H - r} \tag{2}$$

The corresponding restitution coefficients were 0.49 for sand and 0.078 for rubber. Substituting the results to Eq. (1) to obtain the damping ratio, the results were 0.22 and 0.63 for sand and rubber, respectively. The standard deviation for silica beads and rubber beads was found to be 0.3 and 0.16, respectively, suggesting excellent agreement of the tests.

A three-dimensional simulation of the restitution test was also performed by using numerical software Particle Flow Code (PFC) 3D. The purpose of the simulation was to evaluate the materials' restitution heights under the influence of granular micro-properties such as the damping ratio, material density or stiffness. For each sphere, different damping ratios ranging from 0 to 1 were considered. Actual material densities, such as ρ=1,300 kg/m³ and 2,600 kg/m³, respectively, were selected as input values. For each density value, various contact types and contact stiffness values were compared, including the linear contact model with effective modulus E=1×10^7 Pa and 1×10^9 Pa, respectively, and the Hertz contact model with shear modulus G=3×10^7 Pa, Poisson's ratio ν=0.5, and G=3×10^{10} Pa, ν=0.3, respectively. The same particles size and releasing height were used in the numerical simulation. The restitution coefficient α, as defined in Eq. (2), is plotted about the damping coefficient ζ and other parameters. This is shown in Figure 5.

In Figure 5, the numerical result fits well with the analytical prediction from Eq. (1). It is thus evident that the damping ratio ζ is independent from factors such as contact type, stiffness values or densities, and that the only influence on the damping ratio is its restitution height. The numerical–analytical comparison provides evidence that contact damping between particles and the base surface can be directly obtained from the above calibration. The relevant results are discussed in the DEM model results.

One could argue that material shape or size may create different results. However, it is noted that the rebound height of silica beads is around five times of that of rubber beads, as observed in the test that the irregular and smaller sized rubber and sand beads are used. This can be visually observed but is difficult to capture using the camera. It is much easier to capture the restitution height of spheres because the irregular ones may bounce in different directions. Also, the spheres were simulated numerically, in order to provide consistency for this experiment.

Angle of Repose

The repose angle test was performed in this study to investigate material frictional behavior, as there is a strong correlation between surface characteristics and the repose angle (Liu et al. 2012). For a specific material, its frictional behavior contains two parts: sliding friction and rolling friction, which have been well established through numerical studies (Zhou et al. 1999; Yang et al. 2000; Zhou et al. 2001). In the present study, sliding friction indicates Mohr–Coulomb friction, resisting relative translational movement, while rolling friction indicates the ability of particles to rotate, which reflects particle irregularities. However, one test cannot determine two unknowns (i.e., sliding and rolling friction coefficients) so this study adopted previously reported sliding frictions for sand and rubber materials (Patil et al. 2010). The rolling friction coefficient was determined from the repose angle accordingly.

The experiments used granular sand and rubber materials. Both of the materials were sieved between 1.18 mm to 2.36 mm to obtain the same-sized material, because it might have induced significant differences in both the repose angle and the segregation. The mixture was firstly mixed homogeneously and placed in a funnel with a bottom diameter of 15 mm. A bottom plate was removed to allow the particles to drop by force of gravity. The experiment was performed over a glass base, and the distance from the bottom cone to the base was 60 mm. The schematic drawing is shown in Figure 6 (a). Tests were performed for different materials: sand, rubber, and sand–rubber mixture where the two ingredients were equal in volume. The mixture test was conducted to confirm the individual ingredient test results. Each measurement was repeated three times, recording the height and diameter at two directions so that the angle of repose could be determined.

The granular frictional properties are calibrated by using the DEM simulation. The small-scale material pile (Figure 6 (b)) is meaning in respect to the simulations. Firstly, a small number of particles require less time to attain computation stabilization. Also, owing to the granules to be displaced from the funnel, a large pile may induce broader spreads which also require a longer period of processing time. In addition, the pile is significantly larger in scale than the greatest particle size. The pile formation is not subject to a major size effect and the pile dimension satisfies the segregation purpose.

To simulate the shape parameter of the material granules, despite making clumps of the basic shapes of 2D disks or 3D spheres (Indraratna et al. 2012; Chen et al. 2014; Falagush et al. 2015), a rolling resistance behavior at contact could be introduced as suggested by Ai (2010). It has shown great advantages in simulating a stable pile with a finite angle (Zhou et al. 1999; Yang et al. 2000; Zhou et al. 2001). The same technique is used in this simulation. Similar to the Mohr–Coulomb friction theory, the rolling resistance model imposes a granular torque by introducing a rolling friction coefficient f_r. A study of rolling resistance model can be found in Ai (2010).

A calibration process is required to determine the rolling friction coefficient, because very limited research has been focused on the rolling behavior of rubber and sand. The funnel was made by assembling wall plates as two cones, as shown in Figure 6 (b). More than 12,000 spheres particles were used and were first stabilized in the funnel by use of gravity. This was achieved in the simulation by allowing a long simulation time so that the particles' velocity was reduced almost to zero. The bottom plate was removed before particles settled on the base. The input micromechanical parameters are listed in Table 1.

The repose angle cannot be directly measured from the numerical results because there might be systematic errors. For example, the topmost particle may not rest at the center, which induces an inaccurate pile height. Also, as seen in Figure 7 (d), the top of the material pile becomes flat, which underestimates the repose angle. Directly measuring the base radiuses in two directions is also problematic because many particles are scattered. Therefore, an indirect measurement method was developed. As shown in Figure 7 (d), slice the pile horizontally at two elevations: one at the pile's bottom, and the other one at 80% of its apex. The 80% plane was selected to avoid the cone altitude inaccuracy. The angle was determined by measuring the radius of the two slices, and the vertical distance between the slices.

Specifically, the centroid of the funnel is assumed to be the center of the pile bottom rather than the projection of the highest particle at the top. At the chosen height, the upper plane in Figure 7 (d) was used to slice the pile. A number of circles were plot, in equally increasing radius, on the plane, as shown in Figure 7 (b), and were then referred to, in sequence, from ID 1 to N as the radius increased. The circles were used to determine count, C_1, of the particles sitting on the circular plane, as illustrated in Figure 7 (a), as well as count, C_2, of the particles intersecting the circular periphery, as illustrated in Figure 7 (b). Define sphere-intersecting frequency=C_1/C_2. The frequency vs. the sequential circles is illustrated in Figure 7 (c). The upper plane was regarded as the 14th circle because it intersects the maximum number of particles. Similarly the bottom plane sat on the 43th circle. Note that some particles fell outside the circle of preference, e.g., the red sphere in Figure 7 (a) and (b), but intersected at the top with the cut plane. In this circumstance, the elevation and plan views were combined to examine the preferred circle.

Based on calculations and parameters described above, the final results of repose angle were obtained experimentally and numerically. The results are shown in Table 2. Through iteration, the rolling friction coefficients were determined. Different coefficients were determined for the sand and rubber, respectively, as shown in Table 1. Then, when they were mixed at equal volume, the repose angles were examined again, enabling verification of the coefficients through numerical and experimental tests. The results in Table 2 suggest excellent agreement between the numerical and experimental tests. Specifically, for the sand heap, the repose angle is 31.1 ° in the experiment and 31.4 ° in the simulation. Similarly excellent agreement is obtained for the rubber heap and rubber sand mixture heap, verifying the validity of the particle frictions of forming the heaps. At this stage, each single micro parameter has been determined so that digital image processing could be performed.

As a simulation result, it is noted that different groups of material stiffness were used in the simulation but it has negligible impact on the repose angle. Owing to the fact that gravity is the only force considered, the load transmission is negligible at particle contact, so that the impact on the material behavior is minor. The change of material stiffness may have negligible influence to granular behavior for some particular cases. For example, Chung

(2006) studied rod penetration and identified that scaling inter-particle contact stiffness did not show any significant variations on the simulation results, but provided considerable simulation efficiency. It was concluded that the main reason was that reducing stiffness has only minor effects on load transmission onto the boundary surfaces. Ai (2010) illustrated the same finding for stiffness scaling, but argued that if the stiffness is scaled too low, it may result in unstable behavior for a granular pile. This specified methodology was also adopted by Shi et al. (2007) because it has no essential effect on flow mechanics.

Segregation Observation

Segregation was observed in both the numerical simulation and the experimental test. Figure 8 (a) and (b) show material piles in elevation view from the experimental and numerical studies, respectively. The rubber and sand beads are represented as green and blue spheres respectively in the numerical simulations. In addition to the similarity in the repose angle, it is also clear that the pile surfaces are mostly covered by rubber material. A similar surface covering can be seen in the plan view as well (Figure 8 (c)) and (d)), demonstrating verification of the numerical results. Further quantitative comparison is provided in the subsequent sections.

To gain insight into the inner material distribution, the material piles were sliced horizontally at its mid-height, removing the respective top cone and exposing the heap core. The mid-height core was assumed of representing the particle distribution inside the heaps. The particles on the core were examined. For both the test heap and the simulation heap, the majority of sands stayed in the central area (Figure 8 (e) and (f)). Close agreement exists between the experimental and numerical results in respect to particles distribution on both the heap surface and inner core. Again, this agreement is subject to further quantitative comparison which is accomplished through the digital image processing as follows.

Digital Image Processing

One of the main objectives of this research was to present a measurement method that could be used to quantify the segregation obtained from the experiment and numerical simulation. Despite other method that has been proposed to quantify the segregation, there is a size difference in the mixture. A more general method was developed based on visual comparison between numerical and experimental results (Shi et al. 2007). As an improvement of visual comparison, this can be quantitatively measured by using the digital image processing (DIP) method, which has been applied in many fields, such as identifying soil features (Aydemir et al. 2004; Manahiloh et al. 2016), diagnosing soil–rock mesostructure (Kemeny et al. 1993; Villeneuve et al. 2011), analyzing coarse aggregate shape and size (Yue and Morin 1996; Altuhafi et al. 2013), and measuring saturation degree (Yoshimoto et al. 2011). In this paper, as size effect is not the primary consideration, the DIP method was adopted to quantify and compare material segregation between the numerical simulation and experimental results. Based on the literature review conducted in this study, it is the first time of such comparison has been conducted in rubber–sand segregation testing.

DIP method refers to the process of converting a picture into a digital form, and then analyzing the digital image to acquire the useful, underlying information. In the analysis, a picture is represented by a number of pixels. Each pixel is a combination of primary colors. A standard digital picture often uses the red (R), green (G) and blue (B) channels which can be perceived by human eyes and used in simple computer displays. The information extracted from a digital picture can be expressed as a discrete function on a ($N \times M$) grid, known as an intensity matrix in the Cartesian coordinate system (Yue and Morin 1996):

$$I_k = \begin{bmatrix} I_k(1,1) & I_k(1,2) & \cdots & I_k(1,M) \\ I_k(2,1) & I_k(2,2) & \cdots & I_k(2,M) \\ \vdots & \vdots & & \vdots \\ I_k(N,1) & I_k(N,2) & \cdots & I_k(N,M) \end{bmatrix} \tag{3}$$

where I is a value often refers to the intensity level of a digital image ranging from 1 to 255; k =1 to 3, representing red, green and blue channels, respectively; therefore there are three separate matrixes for an image. The I value extraction process is accomplished by MATLAB which is equipped to read color channel information. The present paper briefly illustrates the method for a colored image analysis in the next section. As the sample heap was formed on a glass plane, and the glass background color was similar to the color of the sample, it was not easy to find the color difference between sand and the background, and rubber and the background. Some pre-treatment was required to change the background color. It was chosen to substitute a blue background for the glass background so that it is easier to select the threshold value for further analysis. Figure 9 (a) was converted from Figure 8 (c) by changing the background color. For convenience, some particles scattered on the glass base were excluded because the amount of these particles are negligible compared to the total granular number.

The threshold value was obtained by processing the pixels of an image. However a high resolution image consists of a large number of pixels (> 15 million). Distinguishing color differences directly from the original picture requires long processing time as a result. For simplification in the detailed analysis, a small-sized picture was extracted as an example so that image processing could be performed. Figure 9 (b) picked up a small region of 35×43 pixels, which contains all important elements of the image.

After selecting the small example image as shown in Figure 9 (b), a detailed analysis was conducted to find threshold values between color regions. MATLAB was used to read individual pixels into I_1 for red, I_2 for green, and I_3 for blue. However, the three values cannot be directly used to map the regions. A solution is to use an HSI system to identify the materials more easily (Chen et al. 2004). The HSI stands for *hue*, *saturation* and *intensity*. According to Chen et al. (2004), this solution combines the above three intensity values based on appropriate weighting, yielding a weighted intensity value, $\boldsymbol{I_w}$. According to NTSC standard for luminance (IBM 1990), $\boldsymbol{I_w}$ is calculated using the following algorithm:

$$I_w = \frac{0.2989 \times I_1 + 0.5870 \times I_2 + 0.1140 \times I_3}{255} \tag{4}$$

where $\boldsymbol{I_w}$ has an interval of [0, 1]. This $\boldsymbol{I_w}$ is also known as grey level intensity in MATLAB, enabling a bi-color image. Based on the $\boldsymbol{I_w}$ values, contours are drawn for the small example image, as shown in Figure 10 (a). Figure 10 (a) clearly identifies the color boundaries of different materials, particularly when compared to the original image (Figure 9 (b)). However, given there may be multiple intensity threshold values, such as between sand and rubber, between sand and the background and between rubber and the background, it was not guaranteed that all color differences have been distinguished. Since the background intensity is a value in between the values of both sand and rubber, the background regions need to be excluded before calculating the image intensity.

Recall the pre-treatment that the background has been pre-dyed to blue; it is easy to find that these regions because they have very high $\boldsymbol{I_3}$ values (for blue channel). In this study, the background part was identified by searching $\boldsymbol{I_3} > 245$ and assigning a very high constant, such as 10,000. Using Eq. (4), the background intensity has a value $\boldsymbol{I_w} > 1$ while the other parts are not affected. In this way, the background is excluded and the only intensity threshold value will be the one between sand and rubber. Based on a trial-and-error method suggested by Chen et al. (2004), a threshold value $\boldsymbol{I_w} = 0.35$ was taken to be the boundary between the partition sand and rubber after comparing multiple values. To yield a clear definition of regions, the pixels with $\boldsymbol{I_w} < 0.35$ were reassigned as a value of 0 (i.e., rubber particles), otherwise a value of 1 (i.e., sand particles). Figure 10 (b) illustrates the intensity contours using the values of 0 and 1. Due to noise influence, such as light intensity, the detection results may not be perfectly correct. However, by comparing Figure 10 (a), (b) and Figure 9 (b), it is believed that $\boldsymbol{I_w} = 0.35$ represents the color boundary between sand and rubber particles and can be applied to the rest part of the image in Figure 9 (a).

RESULTS AND DISCUSSION

This section presents the results from a comparison of the experimental and numerical results for the present study. The material volume ratio can be expressed as the ratio of an area of color based on the intensity threshold outlined earlier. As segregation varies significantly between the inside area and the pile surface, the comparison was made after removing the pile cap, as shown in Figure 8 (e).

Segregation Ratio

Digital image processing is further applied here to calculate the area ratio of different colors. Figure 8 (e) is separated as a peripheral ring and central circle so as to directly compare segregation outside and inside the pile. The comparison between the experiments and simulations is shown in from Figure 11 (a) to Figure 14 (a).

In the test, the radius of the central circle is half of the bottom of the material heap. It is noted that in the numerical analysis, the image has already been presented as basic RGB colors which saves the intensity threshold value selection. The RGB colors represent the three primary colors of red, green and blue. Each pixel of a digital image can be made by the combinations of these primary colors. The calculation of the concentration of sand particles was based on color segmentation, shown in Figure 11 (b) to 14 (b). These figures present grey images obtained using the aforementioned DIP method. In the experiments, the percentage of sand as calculated from a color area in the peripheral ring and the central circle were 32.09% and 69.86%, respectively. While the numerical result showed that blue particles which represent as sand at peripheral ring and central circle are 39.09% and 66.00%, respectively. Excellent agreement is obtained between the test and numerical results. The agreement is supposed to be valid for the rest parts of the heaps, given the heap surface and the core represent the outer and inner particle distribution profiles. The quantitative comparison based on the DIP results shows a close predication of numerical simulation. This comparison is more convincing than visual comparison used in previous studies. Comparing the segregation in both numerical and experimental results also showed that the chosen material properties (i.e., friction, material rolling friction, and damping coefficient) matched the actual material properties. It is suggested that segregation tests can be used as a useful calibration method.

Parametric Study

Due to many input parameters, it is not clear that which parameter had a critical influence on particle segregation. It is necessary to evaluate the impact of each parameter with other parameters unchanged. Table 3 lists possible input values for parameters that potentially affect the segregation. Of the parameters, the rolling and sliding friction coefficients determine the particle surface roughness. Five mixtures are defined, each composed of two materials, *A* and *B*, in equal volume. Again, the mixture ingredients are assumed to be similar in size so that size difference is not considered. In each study, only one parameter was changed while the others remain the same. For example, in case 1, the density for the two ingredients is 2,600 kg/m^3 and 1,300 kg/m^3 respectively while other parameters such as damping ratio or stiffness etc. remain the same, as listed in Table 3. The input values reflect the normal range of materials used as geomaterial ingredients.

The five cases were subjected to the segregation test. The test is similar in process to the aforementioned segregation tests, including forming pile through the funnel, slicing the pile at the mid height to compare the inner core and the outer ring. To assess the segregation, define segregation coefficient, C_s, as suggested by Williams (1976):

$$C_s = \frac{W_I - W_O}{W_I + W_O} \times 100\% \tag{5}$$

where W_I is the volumetric proportion of material *A* in the inner core while W_O is the volumetric proportion of material *A* in the outer ring. Where there is no or negligible segregation, C_s is equal or close to zero, and *vice versa*. The results are provided in Figure 15. It is clear that case 1 stands out, with C_s=17.97% of suggesting the material density governs the segregation. The friction coefficients (or surface roughness) however do marginal effect on the segregation which agrees with results by Pohlman et al. (2006).

Even though the friction coefficients alone do not cause segregation of the material, it has a certain effect on the mixture once there is already a density difference in the mixture. To examine this density–friction combined effect, a new comparison was made between the mixture density ratios ρ_A / ρ_B which increase from 1 to 5, according to different sliding friction values f_s = 0.3, 0.4 and 0.5, respectively. The results are provided in Figure 16. For each case, the segregation coefficient C_s increases with the density ratio. This relationship changes if the material surface roughness increases. The rougher the material surface is, the less likely segregation will happen. Similar findings was observed by Lai et al. (1997) that frictional properties sometimes dominate material segregation such as in the event of long range transport. For the funnel discharge in the current study, the density–friction correlation might be explained as follows: when the surface roughness increases, the mobility of the mixture is affected so that flowing from the funnel requires more kinetic energy and material granules tend to move as a whole. Consequently the mixtures are more difficult to be separated during flow.

CONCLUSIONS

This study presented a DIP method used to examine material segregation based on material color difference. The comparison between the DEM simulation and experiments suggests that DIP could be used as a useful method enabling verification between the DEM and test results.

Material rolling friction and damping ratio for sand and rubber were calibrated by the repose angle and re-bouncing tests, respectively. The parameter values were incorporated into the DEM model for the parametric study. For a uniform mixture, from a microscopic perspective, the density difference had most significant impact to the segregation during the funnel discharge. Other contact properties such as material stiffness, surface roughness or damping ratio had minor to negligible impact. The higher the density difference is, the noticeable the segregation will be. When the segregation needs to be controlled, the material density difference should be considered. However, the density-induced segregation can be offset by the inter-particle friction. The higher the frictional properties are assigned, the less likely the segregation will occur.

ACKNOWLEDGEMENT

This research was funded by the Australian Government through the Australian Research Council.

NOTATIONS

C_1 count of the particles sitting on a cutting plane

C_2 count of the particles intersecting a circular periphery

C_s segregation coefficient

d_r diameter of rubber particle

d_s	diameter of sand particle
E	effective modulus
E_r	effective modulus of rubber particle
E_s	effective modulus of sand particle
f_r	rolling friction
f_s	sliding friction
$f_{r,r}$	rolling friction of rubber particle
$f_{r,s}$	rolling friction of sand particle
$f_{s,r}$	sliding friction of rubber particle
$f_{s,s}$	sliding friction of sand particle
f_w	particle–wall friction
G	shear modulus
h	bead rebound height
H	bead drop height
I	colour channel intensity
I_1	red channel intensity
I_2	green channel intensity
I_3	blue channel intensity
I_w	grey level intensity
k_w	particle–wall stiffness
r	bead radius
W_I	volumetric proportion of material in the inner circle
W_O	volumetric proportion of material in the peripheral ring
α	restitution coefficient
ζ	damping ratio

ζ_r damping ratio of rubber particle

ζ_s damping ratio of sand particle

ν Poisson's ratio

ρ density

ρ_r density of rubber particle

ρ_s density of sand particle

REFERENCES

Ahmed, I., and Lovell, C. (1993). "Rubber soils as lightweight geomaterials." *Transportation Research Record*, (1422), 61-70.

Ai, J. (2010). "Particle scale and bulk scale investigation of granular piles and silos."PhD thesis, The University of Edinburgh, Edinburgh, UK.

Altuhafi, F., O'Sullivan, C., and Cavarretta, I. (2013). "Analysis of an image-based method to quantify the size and shape of sand particles." *Journal of Geotechnical and Geoenvironmental Engineering*, 139(8), 1290-1307.

Anand, A., Curtis, J. S., Wassgren, C. R., Hancock, B. C., and Ketterhagen, W. R. (2010). "Segregation of cohesive granular materials during discharge from a rectangular hopper." *Granular Matter*, 12(2), 193-200.

Aydemir, S., Keskin, S., and Drees, L. (2004). "Quantification of soil features using digital image processing (DIP) techniques." *Geoderma*, 119(1), 1-8.

Bosscher, P. J., Edil, T. B., and Kuraoka, S. (1997). "Design of highway embankments using tire chips." *Journal of Geotechnical and Geoenvironmental Engineering*, 123(4), 295-304.

Chen, C., McDowell, G. R., and Thom, N. H. (2014). "Investigating geogrid-reinforced ballast: Experimental pull-out tests and discrete element modelling." *Soils Found*, 54(1), 1-11.

Chen, S., Yue, Z., and Tham, L. (2004). "Digital image-based numerical modeling method for prediction of inhomogeneous rock failure." *International Journal of Rock Mechanics and Mining Sciences*, 41(6), 939-957.

Chung, Y.-C. (2006). "Discrete element modelling and experimental validation of a granular solid subject to different loading conditions."PhD thesis, The University of Edinburgh, Edinburgh, UK.

Cundall, P. A., and Strack, O. D. (1979). "A discrete numerical model for granular assemblies." *Geotechnique*, 29(1), 47-65.

Donald, M., and Roseman, B. (1962). "Mixing and demixing of solid particles. Part I: Mechanisms in a horizontal drum mixer." *Br Chem Eng*, 7(10), 749-752.

Evans, T., and Valdes, J. R. (2011). "The microstructure of particulate mixtures in one-dimensional compression: Numerical studies." *Granular Matter*, 13(5), 657-669.

Falagush, O., McDowell, G. R., and Yu, H. S. (2015). "Discrete element modeling of cone penetration tests incorporating particle shape and crushing." *International Journal of Geomechanics*, 15(6), 04015003.

Foose, G. J., Benson, C. H., and Bosscher, P. J. (1996). "Sand reinforced with shredded waste tires." *Journal of Geotechnical Engineering*, 122(9), 760-767.

Garga, V. K., and O'shaughnessy, V. (2000). "Tire-reinforced earthfill. Part 1: Construction of a test fill, performance, and retaining wall design." *Canadian Geotechnical Journal*, 37(1), 75-96.

Humphrey, D. N., and Manion, W. P. "Properties of tire chips for lightweight fill." *Proc., Grouting, Soil Improvement and Geosynthetics*, ASCE, 1344-1355.

IBM (1990). "NTSC luminance/chrominance equation definition for digital systems." *IBM Tech Disclosure Bull*, 32(10A), 208-209.

Indraratna, B., Ngo, N. T., Rujikiatkamjorn, C., and Vinod, J. (2012). "Behavior of fresh and fouled railway ballast subjected to direct shear testing: Discrete element simulation." *International Journal of Geomechanics*, 14(1), 34-44.

Itasca (2009). "PFC3D 4.0 User's Manual. ." Itasca Consulting Group, Inc., Minnesota, USA.

Kawaguchi, T., Tanaka, T., and Tsuji, Y. (1992). "Numerical simulation of fluidized bed using the discrete element method: The case of spouting bed." *Trans Jpn Soc Mech Eng Ser B*, 58(551), 79-85.

Kemeny, J. M., Devgan, A., Hagaman, R. M., and Wu, X. (1993). "Analysis of rock fragmentation using digital image processing." *Journal of Geotechnical Engineering*, 119(7), 1144-1160.

Kudrolli, A. (2004). "Size separation in vibrated granular matter." *Reports on Progress in Physics*, 67(3), 209-248.

Kuerbis, R., and Vaid, Y. (1988). "Sand sample preparation-the slurry deposition method." *Soils Found*, 28(4), 107-118.

Lai, P.-Y., Jia, L.-C., and Chan, C. (1997). "Friction induced segregation of a granular binary mixture in a rotating drum." *Physical Review Letters*, 79(25), 4994-4997.

Lee, C., Shin, H., and Lee, J. S. (2014). "Behavior of sand–rubber particle mixtures: Experimental observations and numerical simulations." *International Journal for Numerical and Analytical Methods in Geomechanics*, 38(16), 1651-1663.

Liu, J., Yun, B., and Zhao, C. B. (2012). "Identification and validation of rolling friction models by dynamic simulation of sandpile formation." *International Journal of Geomechanics*, 12(4), 484-493.

Lőrincz, J., Imre, E., Gálos, M., Trang, Q., Rajkai, K., Fityus, S., and Telekes, G. (2005). "Grading entropy variation due to soil crushing." *International Journal of Geomechanics*, 5(4), 311-319.

Manahiloh, K. N., Muhunthan, B., and Likos, W. J. (2016). "Microstructure-based effective stress formulation for unsaturated granular soils." *International Journal of Geomechanics*, 16(6), D4016006.

Masad, E., Taha, R., Ho, C., and Papagiannakis, T. (1996). "Engineering properties of tire/soil mixtures as a lightweight fill material." *Geotech Test J*, 19(3), 297-304.

Nightingale, D. E., and Green, W. P. (1997). "An unresolved riddle: Tire chips, two roadbeds, and spontaneous reactions." *Testing Soil Mixed with Waste or Recycled Materials*, ASTM International, STP1275, 265-285.

Ottino, J., and Khakhar, D. (2000). "Mixing and segregation of granular materials." *Annual Review of Fluid Mechanics*, 32(1), 55-91.

Patil, U., Valdes, J. R., and Evans, T. M. (2010). "Swell mitigation with granulated tire rubber." *Journal of Materials in Civil Engineering*, 23(5), 721-727.

Poh, P. S., and Broms, B. B. (1995). "Slope stabilization using old rubber tires and geotextiles." *Journal of performance of constructed facilities*, 9(1), 76-79.

Pohlman, N. A., Severson, B. L., Ottino, J. M., and Lueptow, R. M. (2006). "Surface roughness effects in granular matter: Influence on angle of repose and the absence of segregation." *Physical Review E*, 73(3), 031304.

Shi, D., Abatan, A. A., Vargas, W. L., and McCarthy, J. (2007). "Eliminating segregation in free-surface flows of particles." *Physical Review Letters*, 99(14), 148001.

Tsang, H. H., Lo, S., Xu, X., and Neaz Sheikh, M. (2012). "Seismic isolation for low‐to‐medium‐rise buildings using granulated rubber–soil mixtures: numerical study." *Earthquake engineering & structural dynamics*, 41(14), 2009-2024.

Villeneuve, M. C., Diederichs, M. S., and Kaiser, P. K. (2011). "Effects of grain scale heterogeneity on rock strength and the chipping process." *International Journal of Geomechanics*, 12(6), 632-647.

Watabe, Y., Shinsha, H., Yoneya, H., and Ko, C. J. (2014). "Description of partial sandy layers of dredged clay deposit using penetration resistance in installation of prefabricated vertical drains." *Soils Found*, 54(5), 1006-1017.

Williams, J. C. (1976). "The segregation of particulate materials. A review." *Powder Technology*, 15(2), 245-251.

Yang, R., Zou, R., and Yu, A. (2000). "Computer simulation of the packing of fine particles." *Physical Review E*, 62(3), 3900-3908.

Yoshimine, M., and Koike, R. (2005). "Liquefaction of clean sand with stratified structure due to segregation of particle size." *Soils Found*, 45(4), 89-98.

Yoshimoto, N., Orense, R. P., Tanabe, F., Kikkawa, N., Hyodo, M., and Nakata, Y. (2011). "Measurement of degree of saturation on model ground by digital image processing." *Soils Found*, 51(1), 167-177.

Yue, Z. Q., and Morin, I. (1996). "Digital image processing for aggregate orientation in asphalt concrete mixtures." *Can J Civil Eng*, 23(2), 480-489.

Zhou, Y., Wright, B., Yang, R., Xu, B., and Yu, A. (1999). "Rolling friction in the dynamic simulation of sandpile formation." *Physica A: Statistical Mechanics and its Applications*, 269(2), 536-553.

Zhou, Y., Xu, B., Yu, A., and Zulli, P. (2001). "Numerical investigation of the angle of repose of monosized spheres." *Physical Review E*, 64(2), 021301.

Zornberg, J. G., Cabral, A. R., and Viratjandr, C. (2004). "Behaviour of tire shred sand mixtures." *Canadian Geotechnical Journal*, 41(2), 227-241.

Figure Captions List

Figure 1 Schematic of DEM model.

Figure 2 Rubber and silica beads used in the damping ratio calibration.

Figure 3 Maximum restitutive height captured by high resolution camera for silica bead and rubber bead.

Figure 4 Restitution height for silica and rubber beads.

Figure 5 The relationship between the damping coefficient and the restitution coefficient with various material properties.

Figure 6 Repose angle test setup: (a) experimental schematic drawing, and (b) numerical simulation.

Figure 7 The numerical measurement of the repose angle: (a) elevation view (not to scale), (b) plan view (not to scale), (c) frequency of particles intersecting the periphery, and (d) sample pile.

Figure 8 Segregation of mixture pile.

Figure 9 Calibration of the digital image: (a) sample pile, and (b) an example image.

Figure 10 Intensity contours expressed as: (a) the color map, and (b) the binary map.

Figure 11 Color segmentation of sand pile at peripheral ring (experiment).

Figure 12 Color segmentation of sand pile at central circle (experiment).

Figure 13 Color segmentation of sand pile at peripheral ring (numerical).

Figure 14 Color segmentation of sand pile at central circle (numerical).

Figure 15 Segregation coefficient for varying mixtures.

Figure 16 Segregation coefficient vs. mixture density ratio under different frictions.

List of Tables

Table 1. Input parameters used in simulation.

Parameter	Value
Diameter of sand particle, d_s, mm	1.54 – 2
Diameter of rubber particle, d_r, mm	1.54 – 2
Density of sand particle, ρ_s, kg/m^3	2,600
Density of rubber particle, ρ_r, kg/m^3	1,300
Sliding friction of sand particle, $f_{s,s}$ *	0.31
Sliding friction of rubber particle, $f_{s,r}$ *	0.6
Rolling friction of sand particle, $f_{r,s}$ #	0.7
Rolling friction of rubber particle, $f_{r,r}$ #	0.6
Effective modulus of sand particle, E_s , Pa	1×10^7
Effective modulus of rubber particle, E_r, Pa	1×10^5
Particle – wall friction, f_w	0.405
Particle – wall stiffness, k_w	1×10^6
Damping ratio of sand particle, ζ_s #	0.63
Damping ratio of rubber particle, ζ_r #	0.22

* data from Patil et al. (2010); # data from calibration.

Table 2 Measurement of repose angle.

	Experiment							Simulation
		Height	Diameter (mm)				Average	
Sample	Test	(mm)	*X*	*Y*	Average	Angle (°)	angle (°)	Angle (°)
Sand bead	1	28	88	92	90	31.9	31.1	31.4
	2	34.5	118	117	117.5	30.4		
	3	35	112	120	116	31.1		
Rubber bead	1	39	103	105	104	36.9	36.3	36.5
	2	40	108	108	108	36.5		
	3	34	95	96	95.5	35.5		
Mixture	1	39	108	106	107	36.1	35.0	34.8
	2	34	100	102	101	34.0		
	3	35	101	100	100.5	34.9		

Table 3 Material properties used in the parametric study.

Case	Ingredient	Density (kg/m³)	Damping ratio	Stiffness (kPa)	Rolling friction coefficient	Sliding friction coefficient
Case 1	*A*	2,600	0.2	1×10^5	0.6	0.3
	B	1,300	0.2	1×10^5	0.6	0.3
Case 2	*A*	1,300	0.2	1×10^5	0.6	0.3
	B	1,300	0.4	1×10^5	0.6	0.3
Case 3	*A*	1,300	0.2	1×10^7	0.6	0.3
	B	1,300	0.2	1×10^5	0.6	0.3
Case 4	*A*	1,300	0.2	1×10^5	0.3	0.3
	B	1,300	0.2	1×10^5	0.6	0.3
Case 5	*A*	1,300	0.2	1×10^5	0.6	0.3
	B	1,300	0.2	1×10^5	0.6	0.6

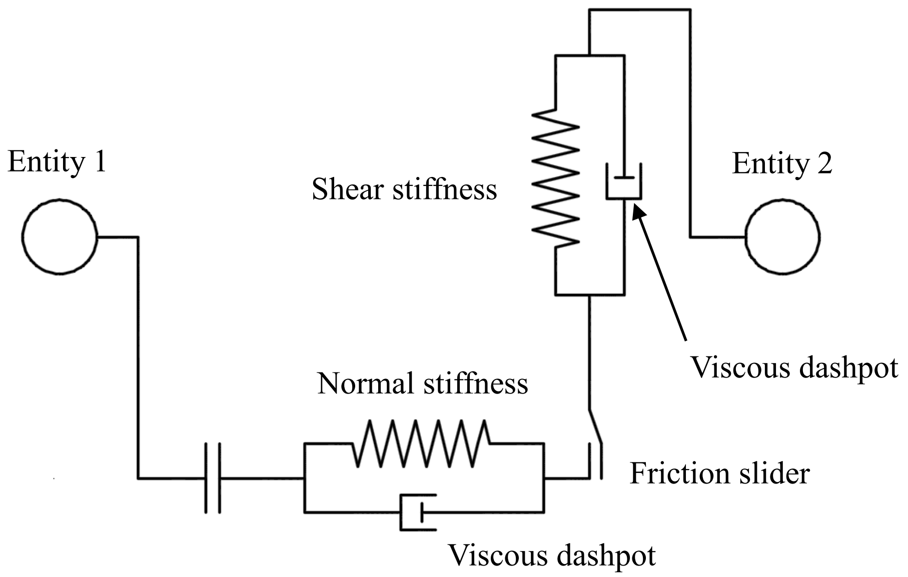
Entity 1
Shear stiffness
Entity 2
Viscous dashpot
Normal stiffness
Friction slider
Viscous dashpot

Figure 2 Click here to download Figure Fig 2.tif

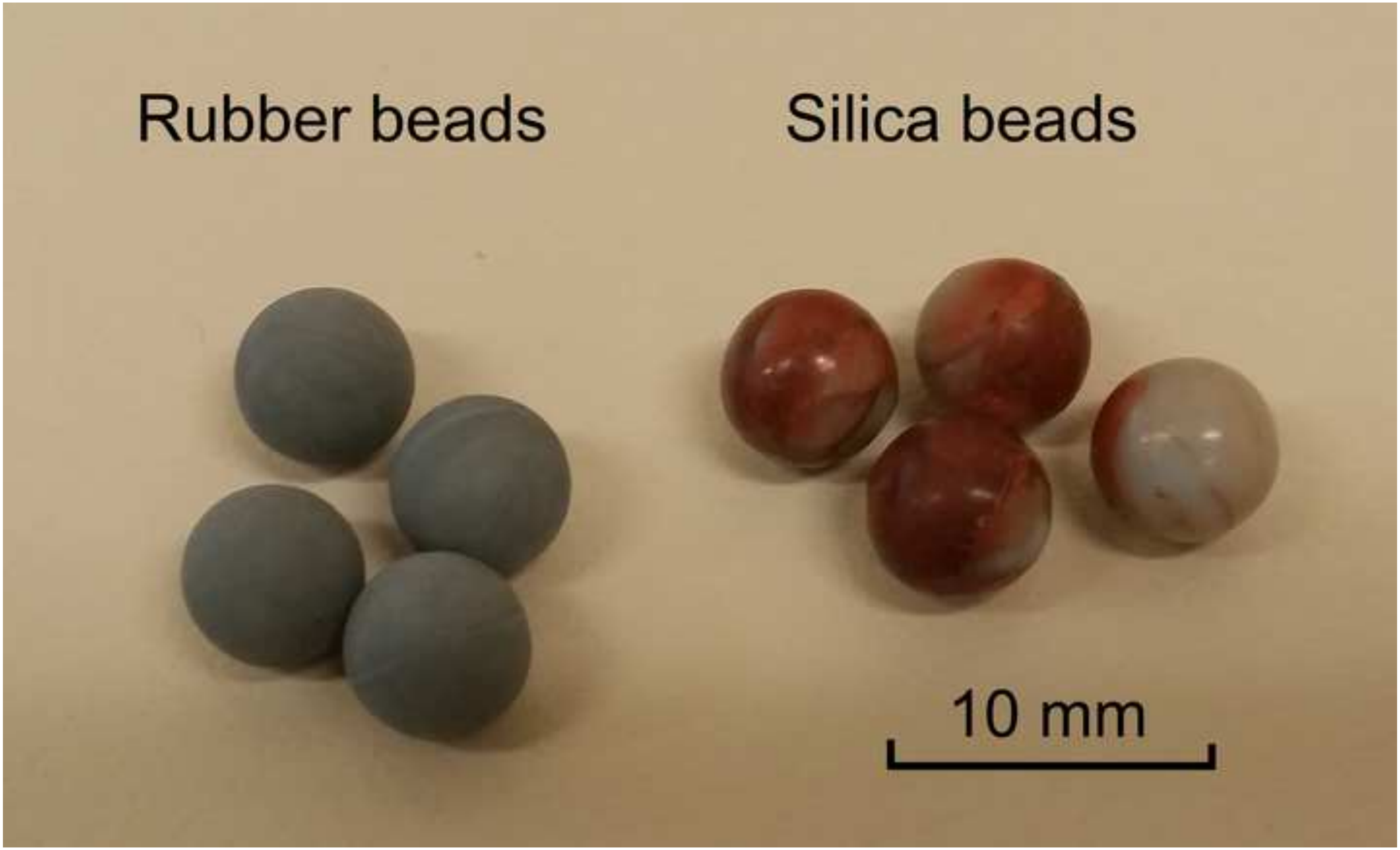

Figure 3a

Click here to download Figure Fig 3a.tif

Figure 3b

Click here to download Figure Fig 3b.tif

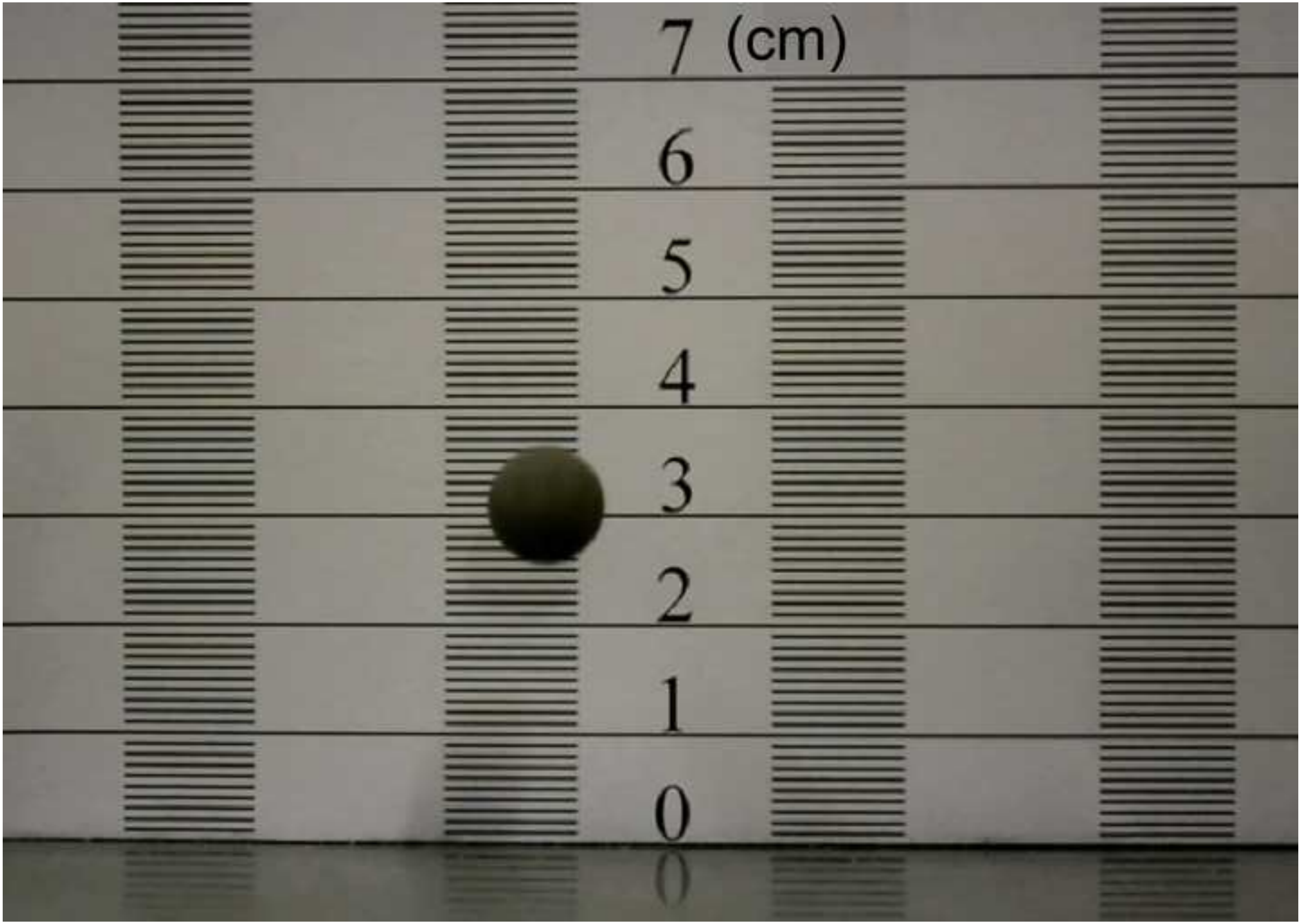

Figure 4 Click here to download Figure Fig 4.docx

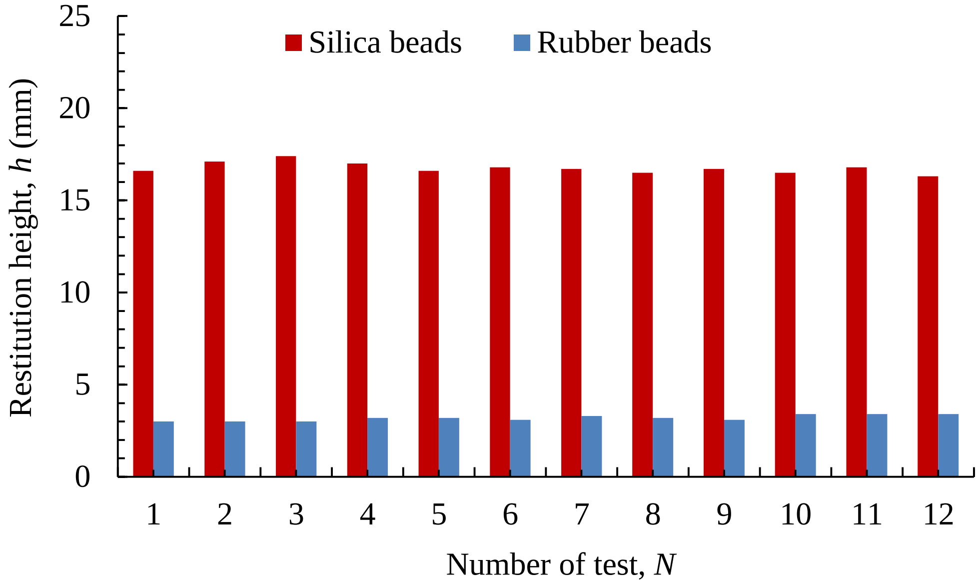

Figure 5

Click here to download Figure Fig 5.pdf

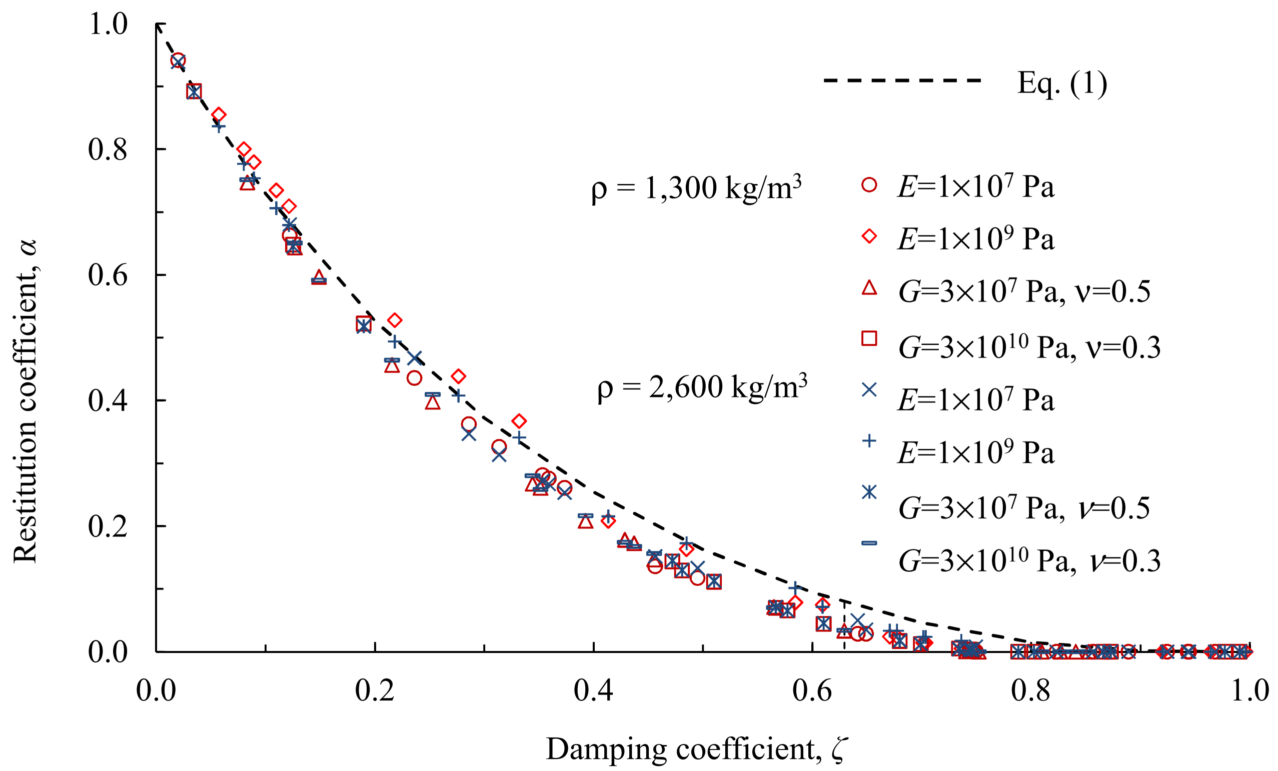

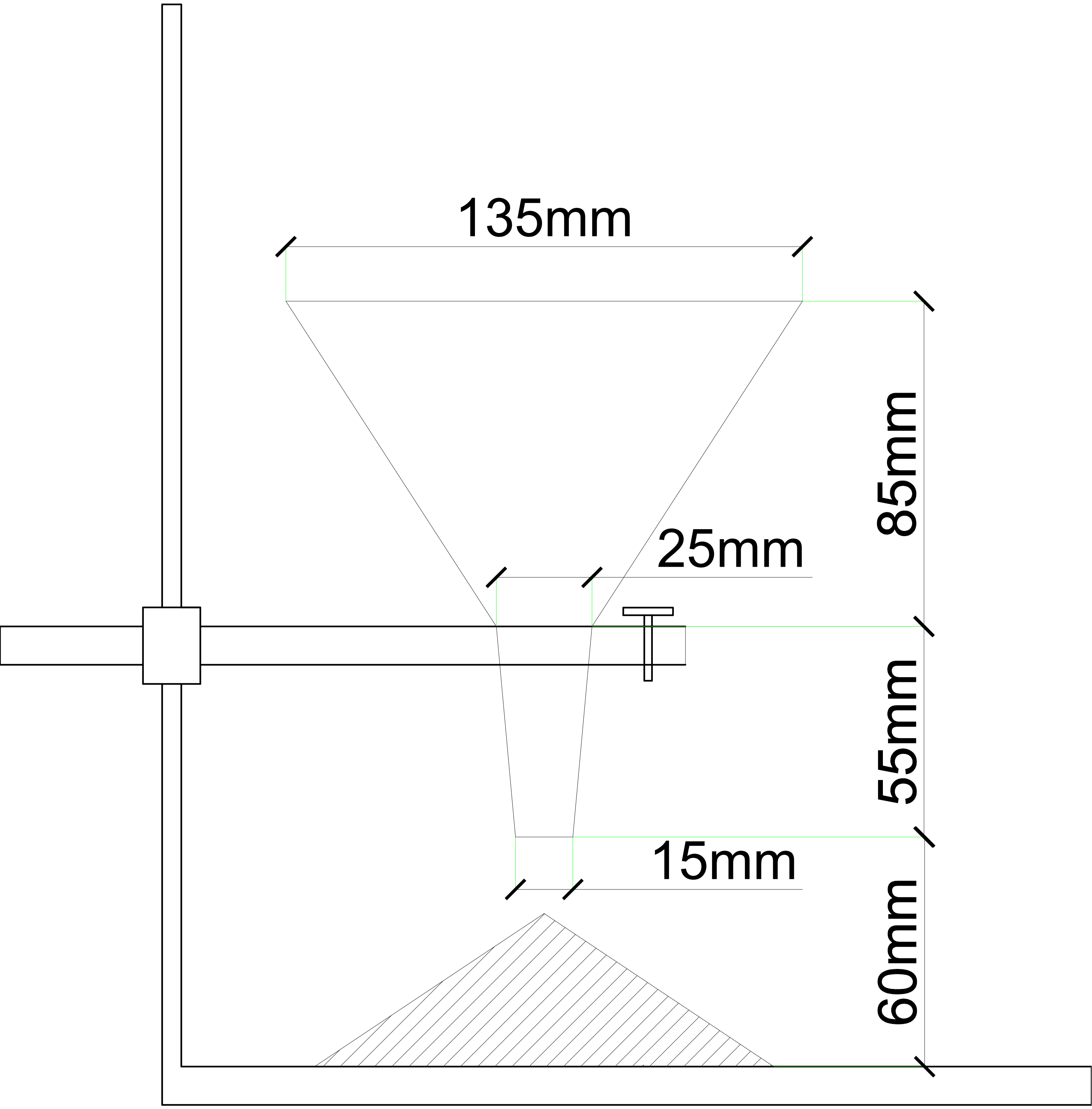
135mm
25mm
15mm
85mm
55mm
60mm

Figure 6b

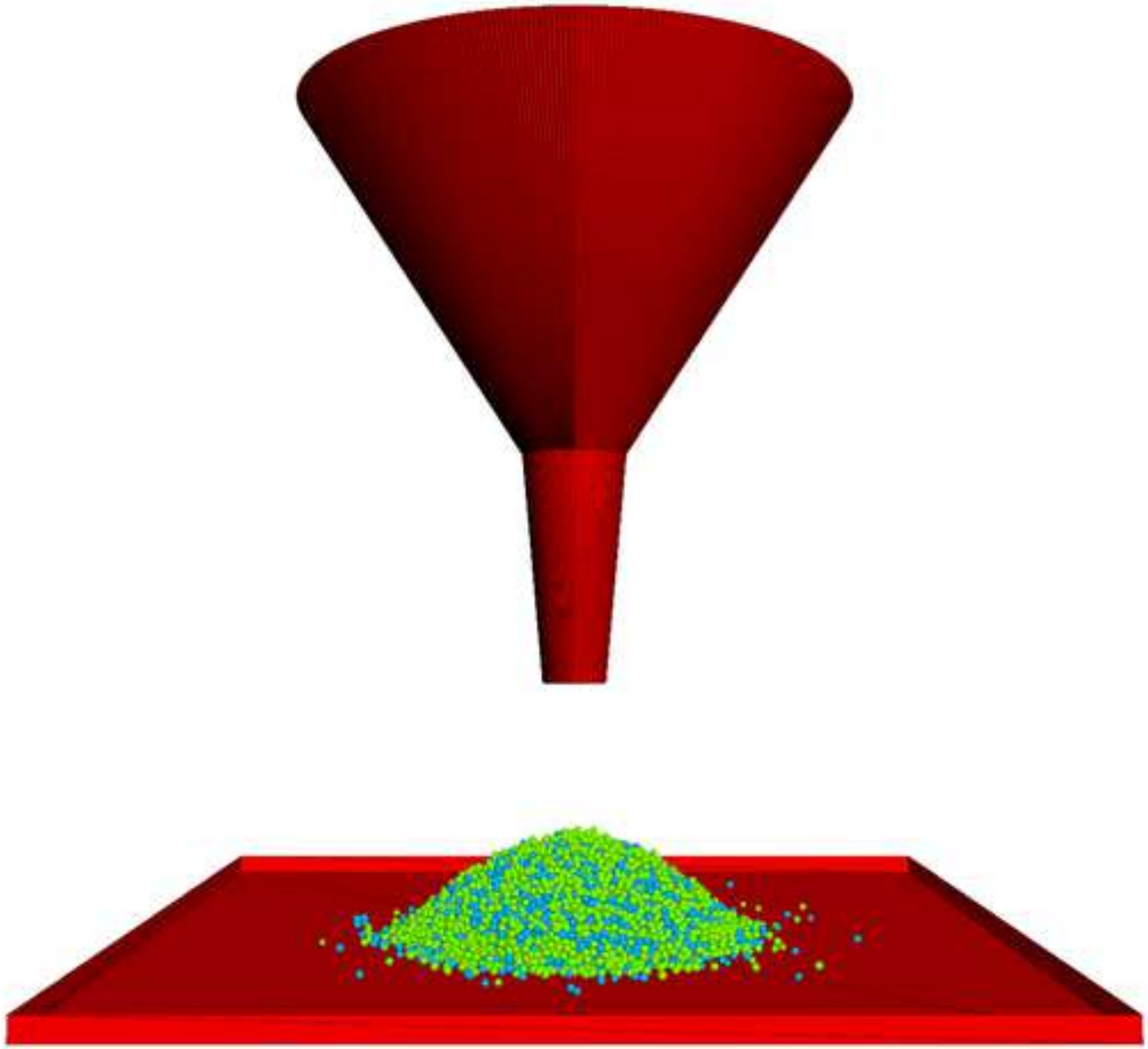

Figure 7(a-b)

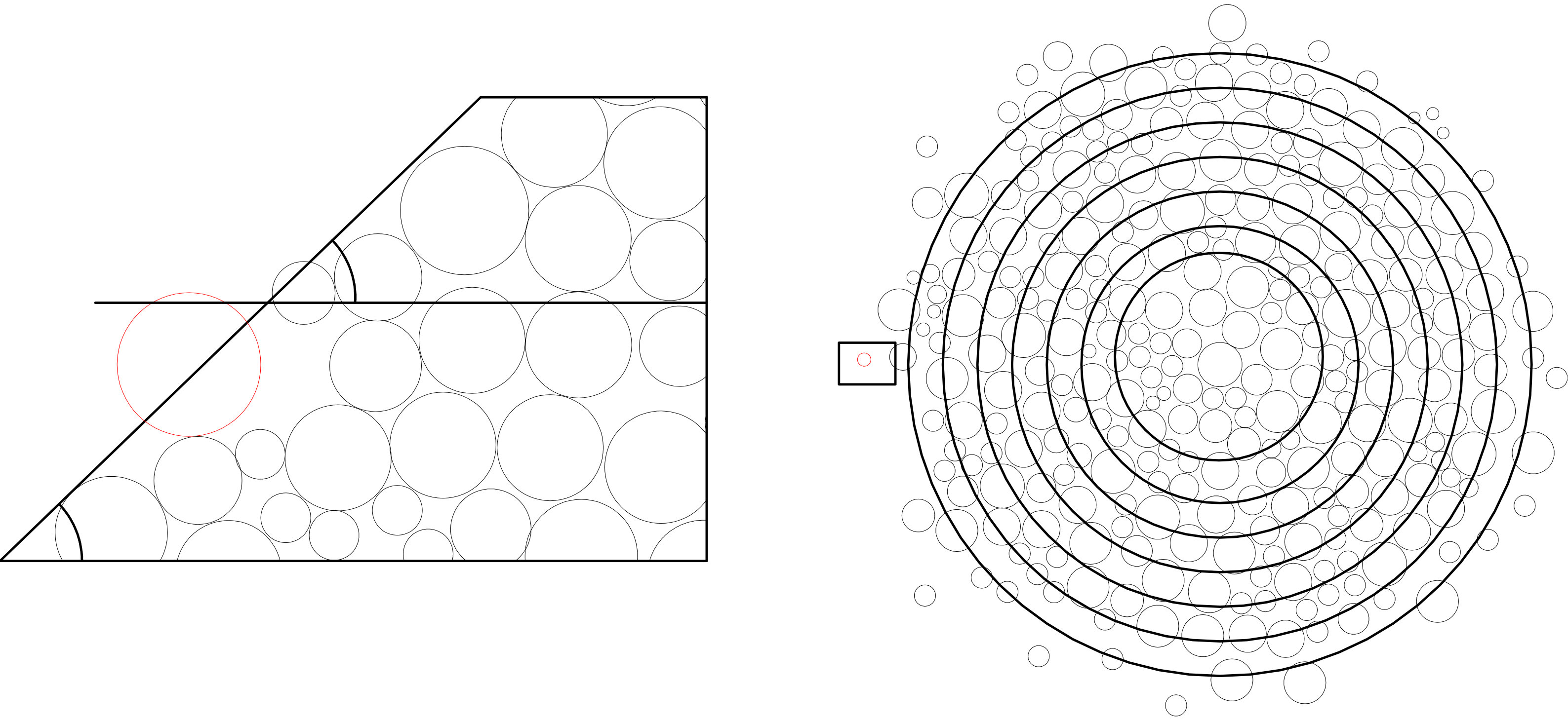

Figure 7c

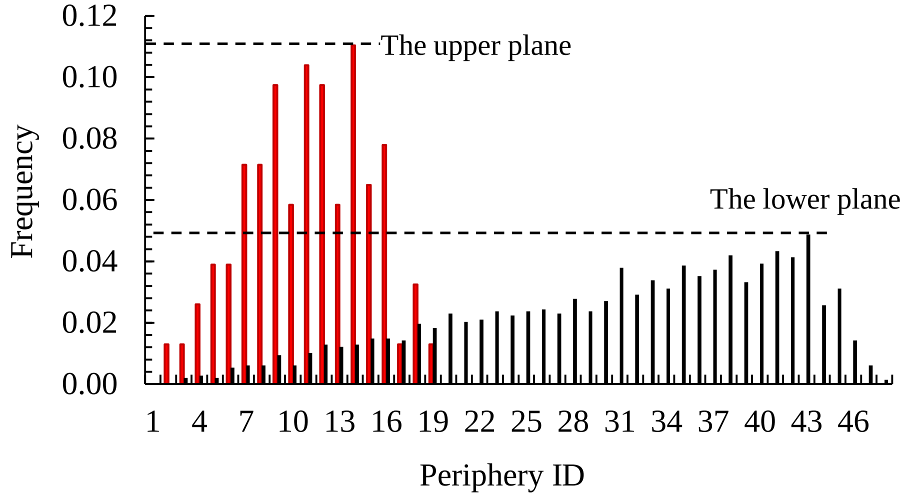
Frequency
0.12
0.10
0.08
0.06
0.04
0.02
0.00
The upper plane
The lower plane
1 4 7 10 13 16 19 22 25 28 31 34 37 40 43 46
Periphery ID

Figure 7d

Click here to download Figure Fig 7d.tif

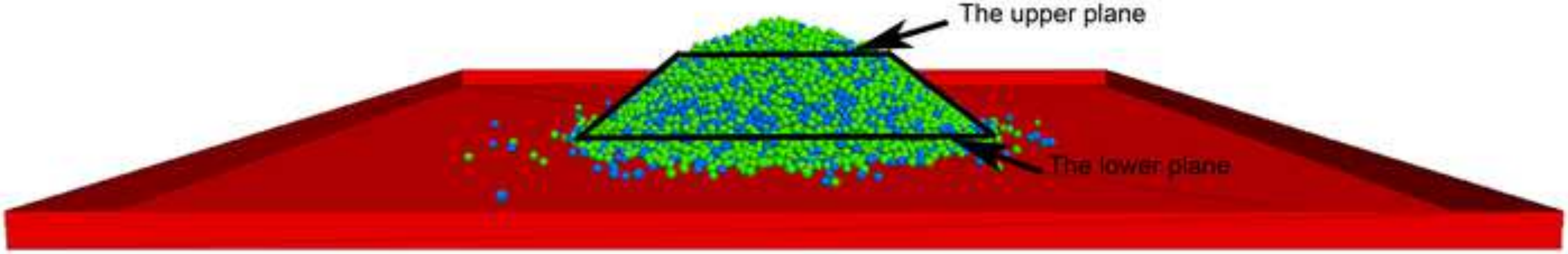

Figure 8a

Click here to download Figure Fig 8a.tif

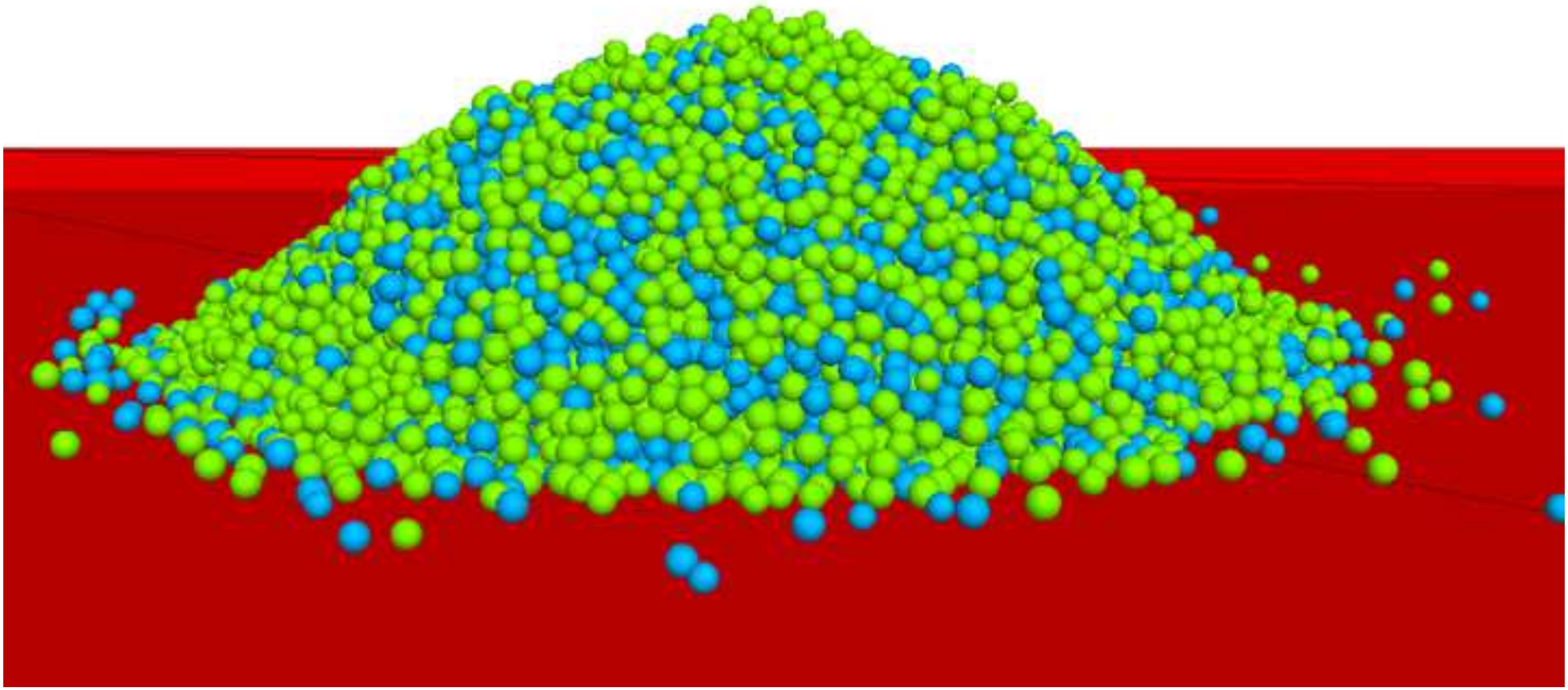

Figure 8c

Click here to download Figure Fig 8c.tif

Figure 8d

Click here to download Figure Fig 8d_2.tif

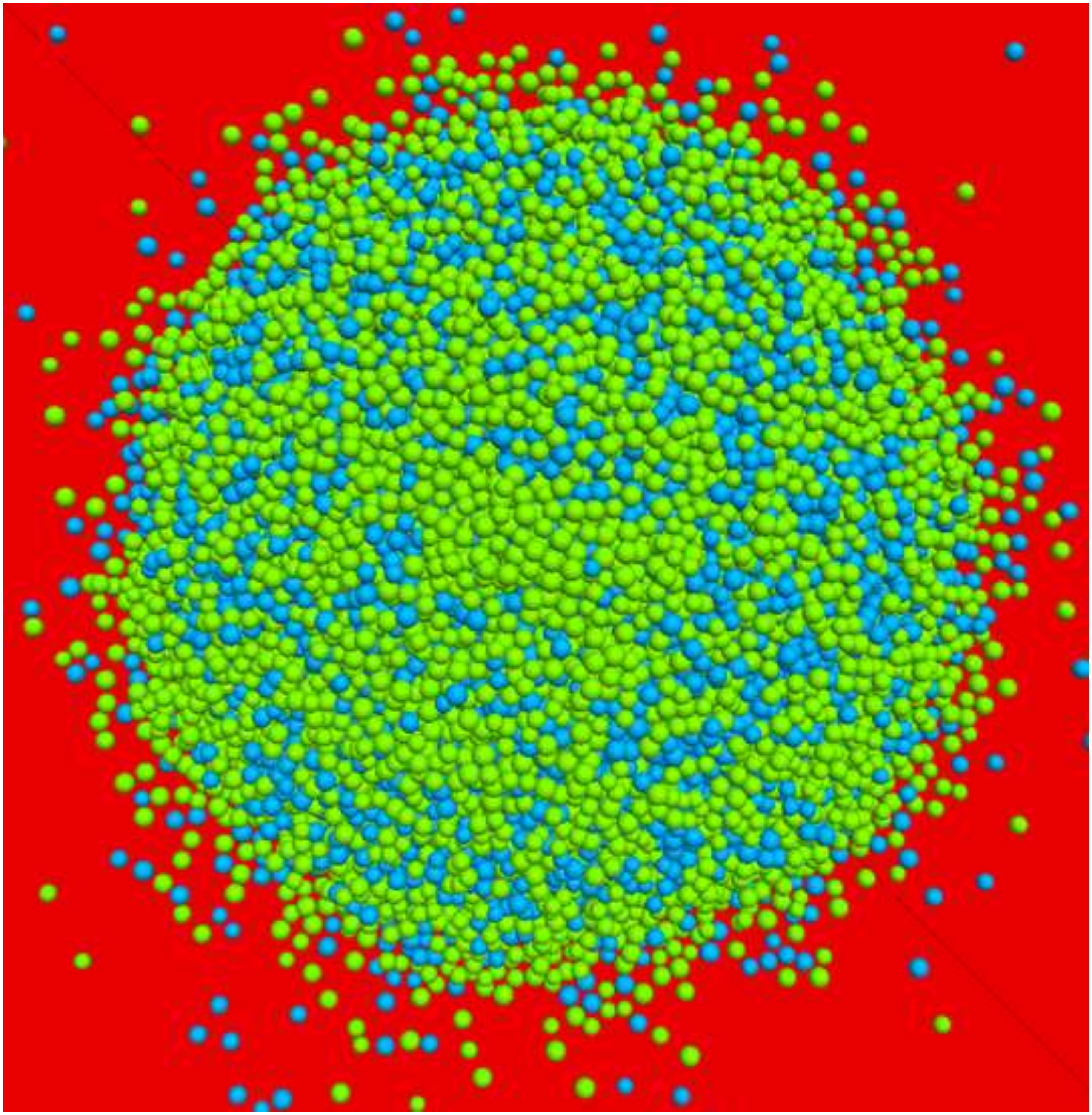

Figure 8e

Figure 8f

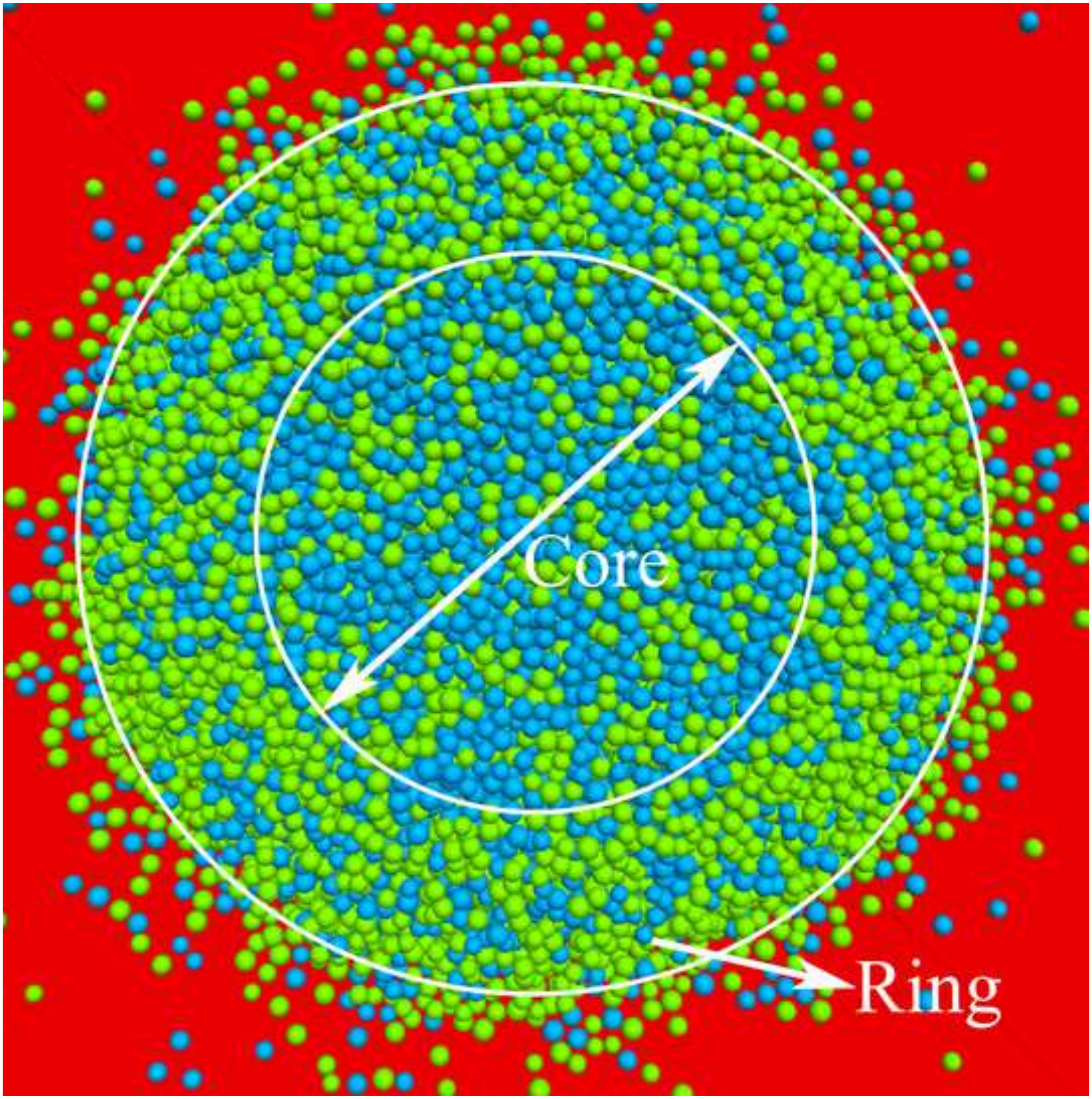

Figure 9a

Click here to download Figure Fig 9a.tif

Figure 9b

Click here to download Figure Fig 9b.tif

Figure 10a

Click here to download Figure Fig 10a.tif

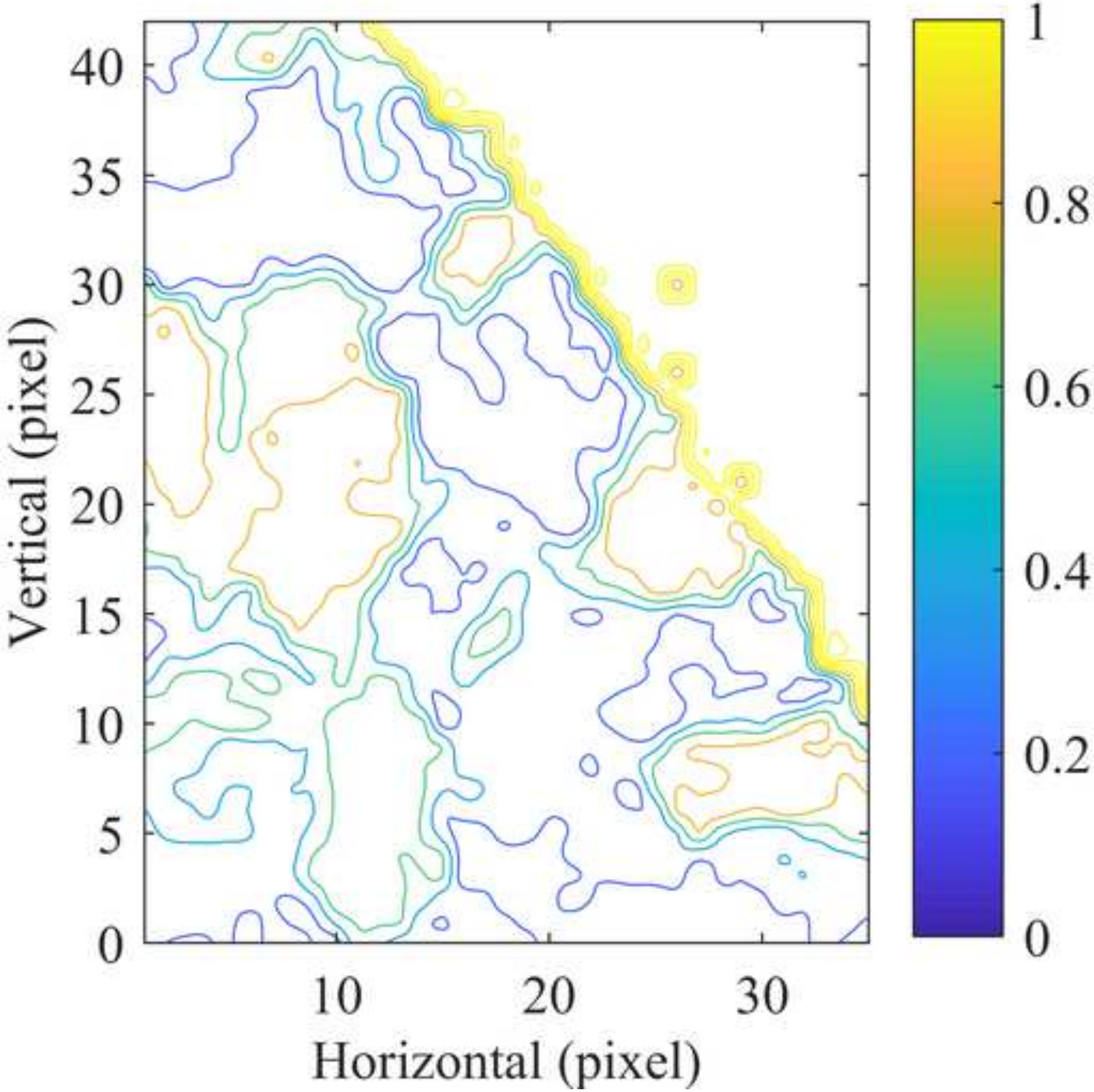

Figure 10b

Click here to download Figure Fig 10b.tif

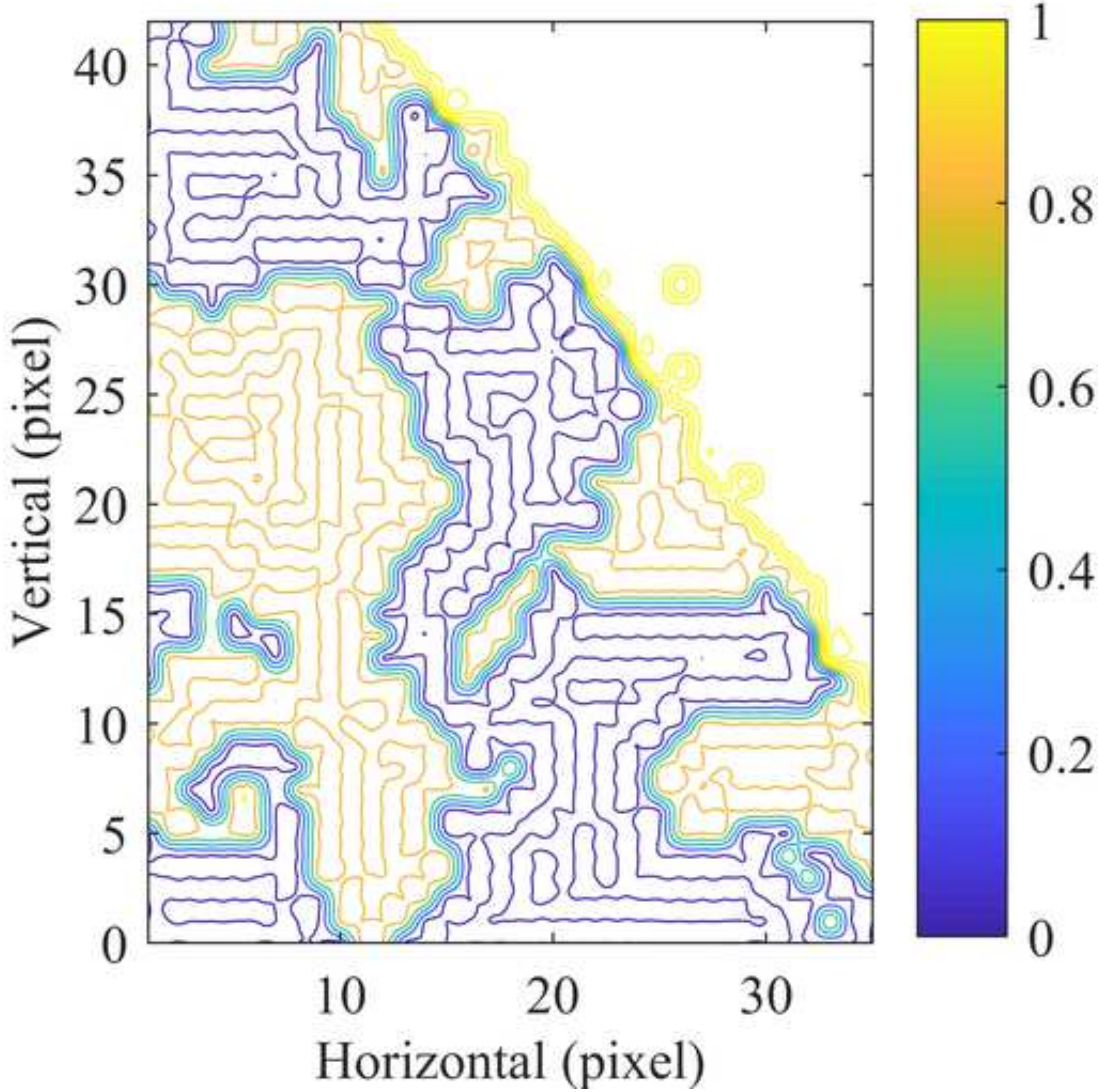

Figure 11a

Click here to download Figure Fig 11a_2.pdf

Figure 11b

Click here to download Figure Fig 11b_2.tif

Figure 12a

Figure 12b

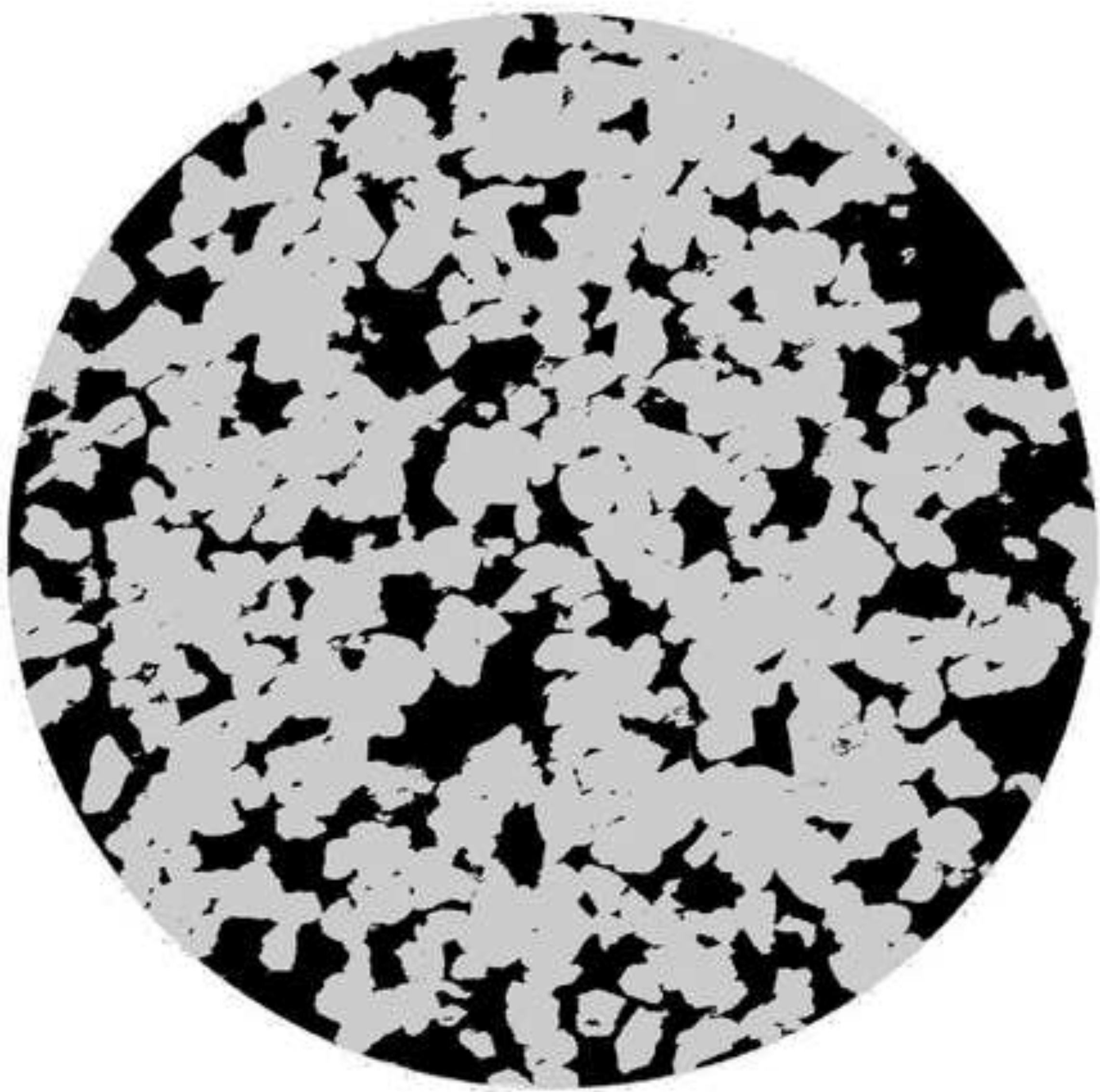

Figure 13a

Click here to download Figure Fig 13a.tif

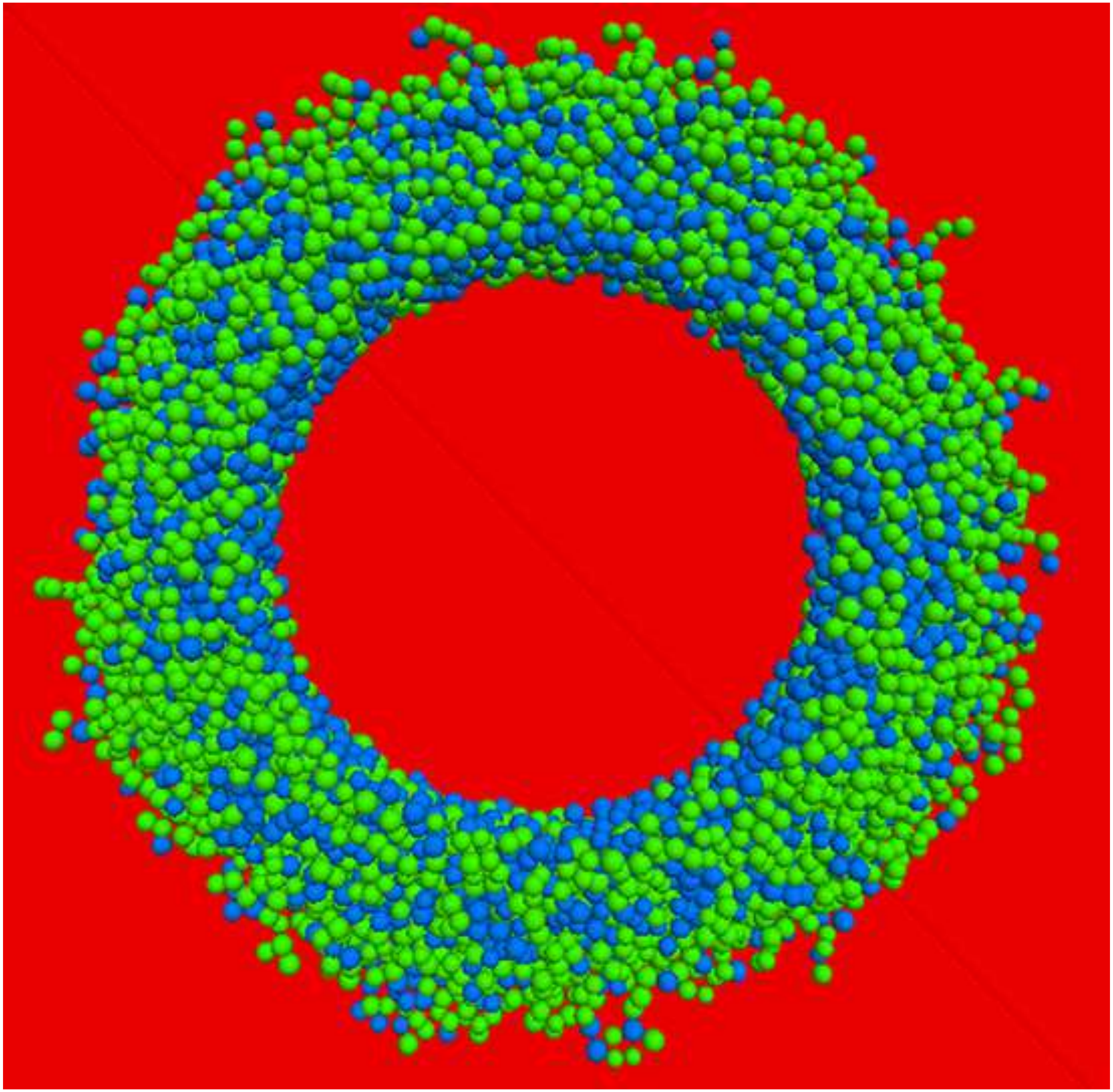

Figure 13b

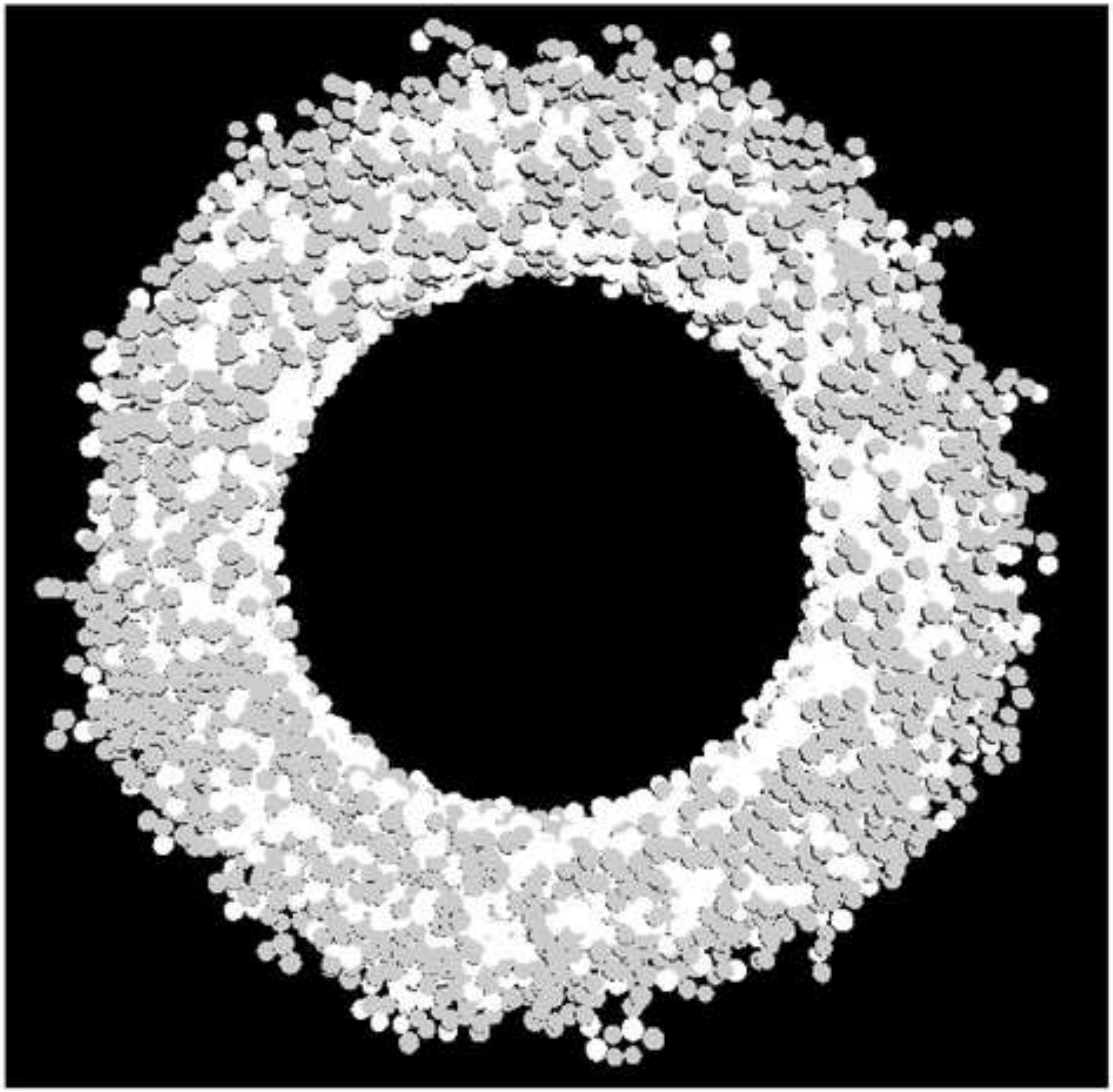

Figure 14a

Click here to download Figure Fig 14a_2.tif

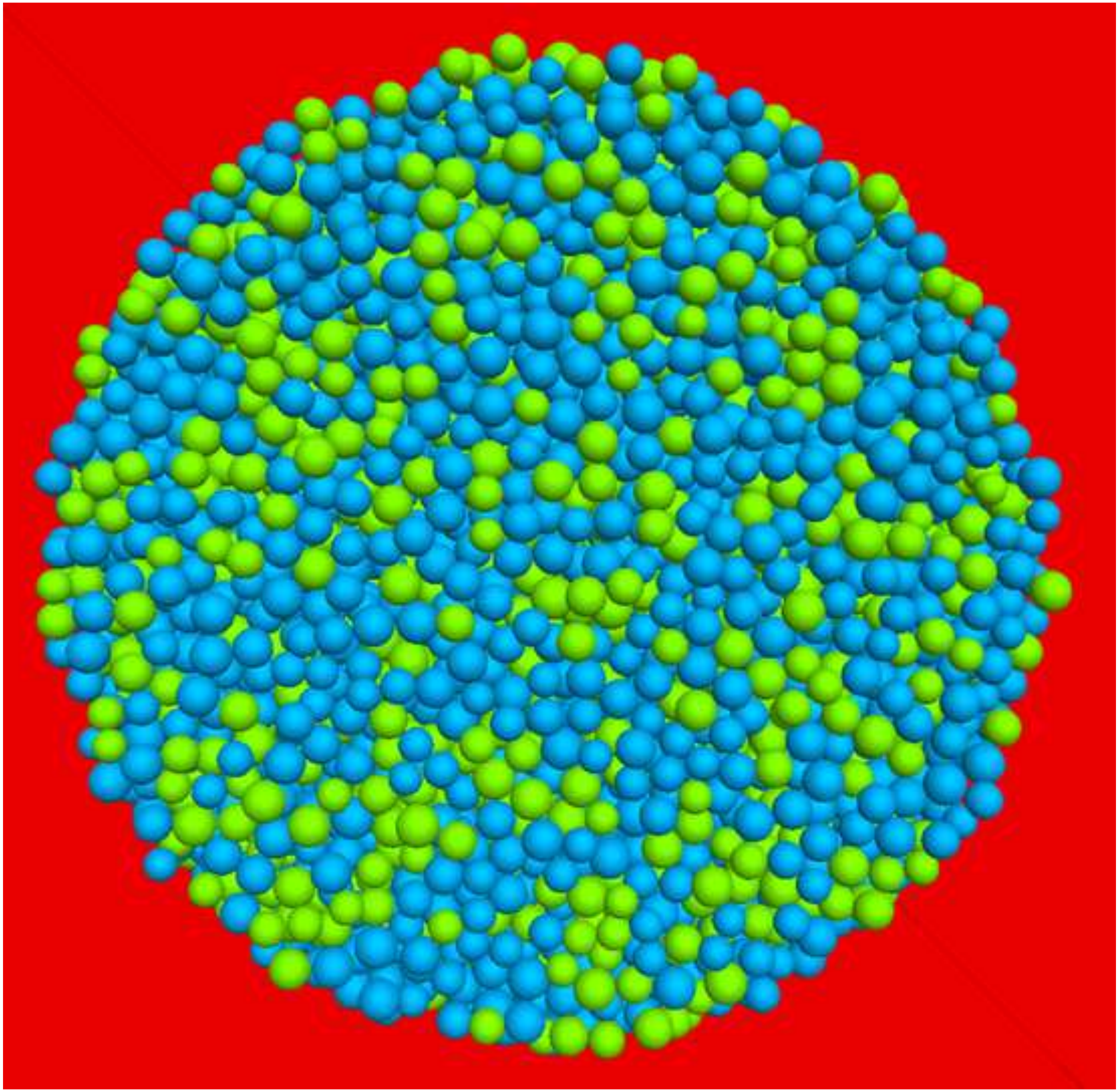

Figure 14b

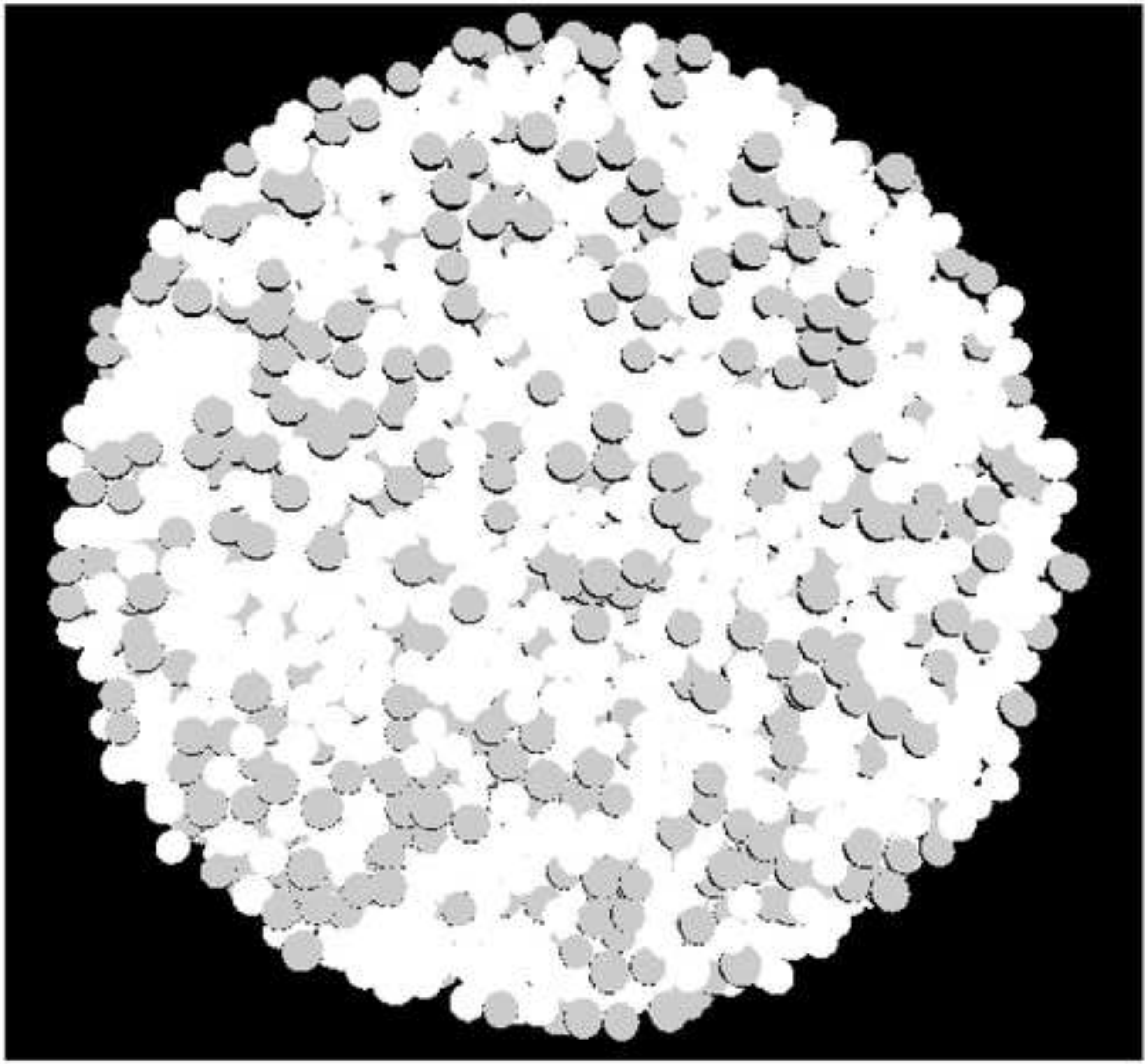

Figure 15 Click here to download Figure Fig 15.pdf

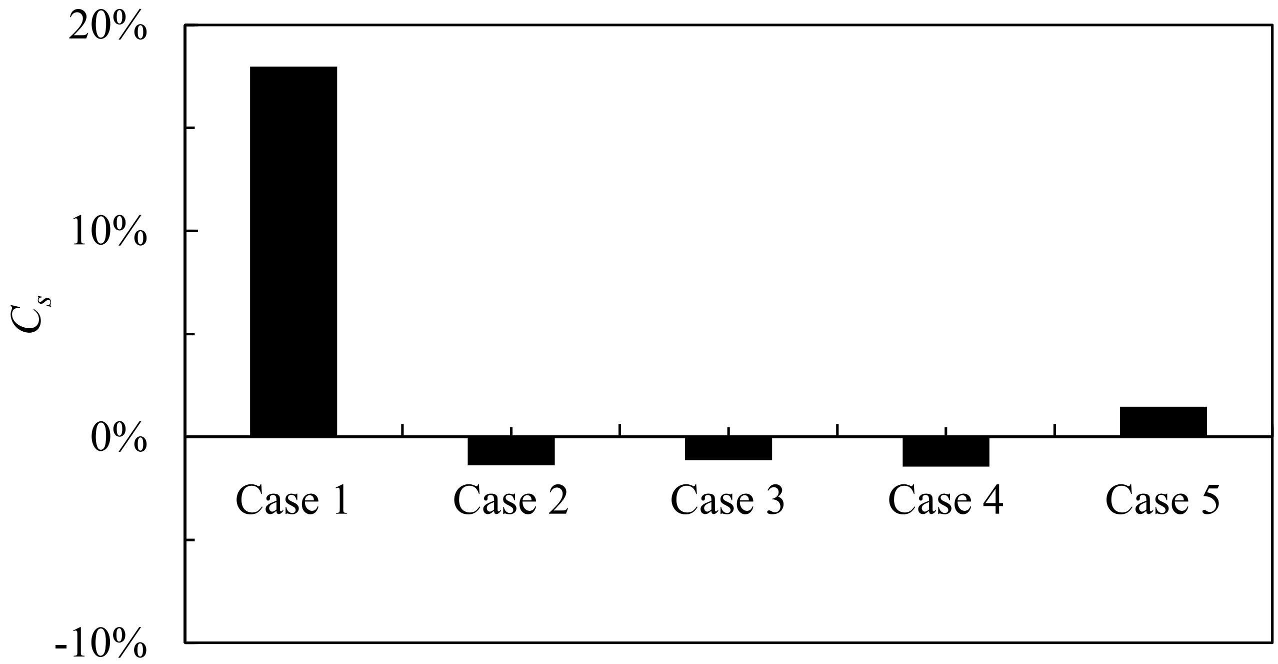

Figure 16

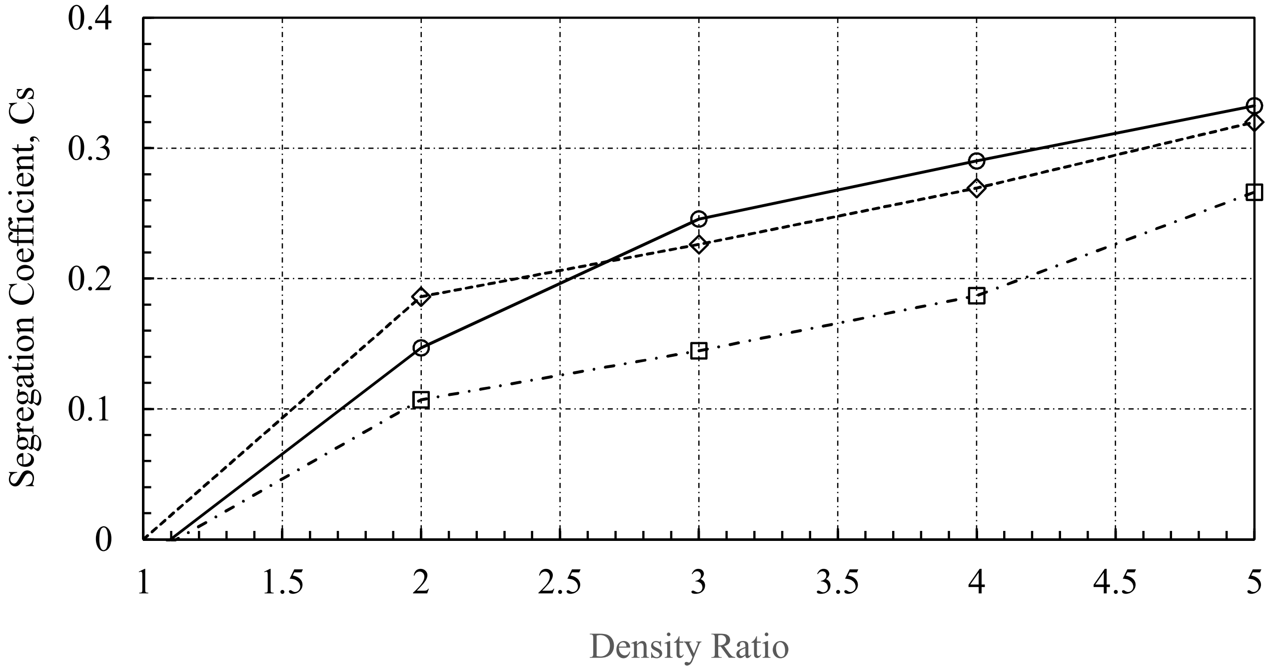

0.4
0.3
0.2
0.1
0
Segregation Coefficient, Cs
1
1.5
2
2.5
3
3.5
4
4.5
5
Density Ratio